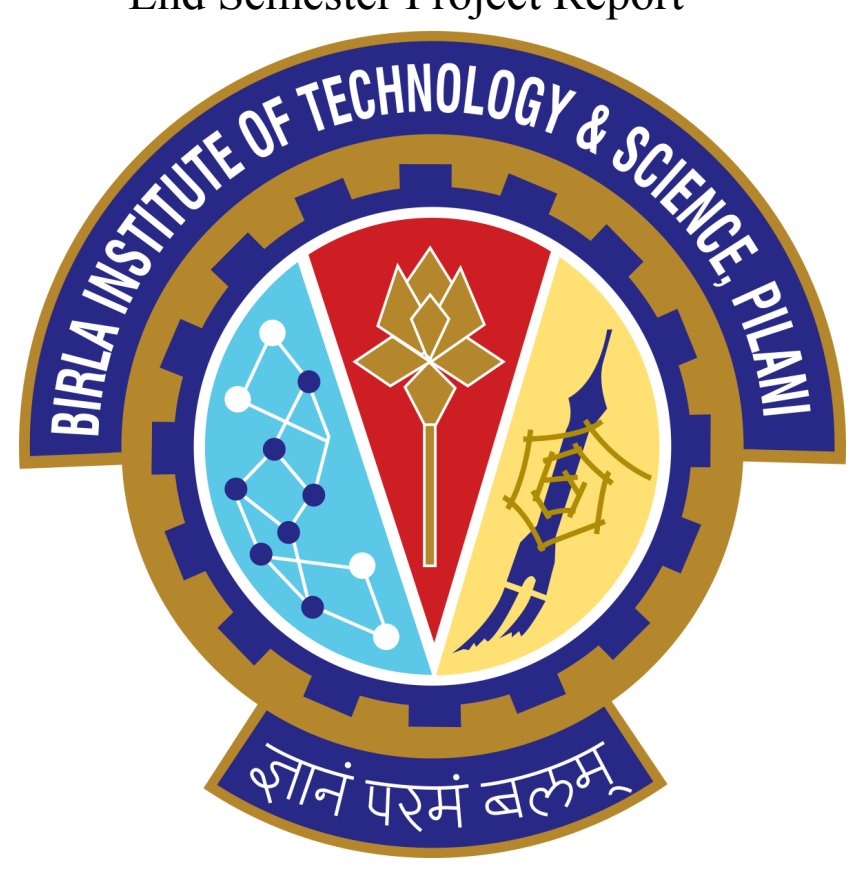
# End Semester Project Report



# Design Oriented Project (ME F376)

Topic: Investigating the Crashworthiness Performance of Crash Box Fabricated from Various Aluminium Alloys under the action of Uniaxial Compressive Loads

Under the guidance of
Dr. Kiran Dinkar Mali
Assistant Professor, Department of Mechanical Engineering
BITS - Pilani, K. K. Birla Goa campus

Members:	ID No:
V. Priyal	2017B1A40819G
Devesh M. Dimble	2017B4A40052G
Abhinav Kumar Pawan	2018A4PS0501G

# **Abstract**

A vehicle's crashworthiness represents the ability of a vehicle structure and any of its components to absorb the crash energy during a collision such that the injury caused by external loads on the occupants are within the limits given by the motor vehicle safety standards. The main components of the vehicle structure involved in absorbing the crash energy are bumpers. structural beams and crash boxes (tubes). Crash boxes are responsible for absorbing the most amount of crash energy among any other structural components in a vehicle and are incorporated with other structural members like bumpers. Since they are located after the bumpers, they are the first to absorb this impact energy in a way that they undergo progressive deformation (or buckling). Over the years of advancing research, crash boxes have gained significant importance in the field of vehicle crashworthiness. These energy absorbers have been the subject of numerous experimental and numerical studies, mainly with the aim of finding an optimal mix of their performance parameters based on their different materials, mechanical properties and geometric features. Generally, these parameters on which the performance of these crash boxes are assessed are peak force, mean force, crush force efficiency, energy absorption and specific energy absorption. As their performance parameters are mainly dependent on their mechanical properties which comes from the material used for their manufacturing, the decision of choosing the appropriate material has always been the center of the problem.

In this report, an attempt has been made to assess the crushing performance of different wrought aluminium (alloy) grades under quasi-static uniaxial compression based on the above mentioned parameters by carrying out numerical simulations in ABAQUS/ explicit software which makes use of the finite element method to obtain the results. The choice of taking wrought aluminium grades for this analysis was made by looking at its cost effectiveness and formability during manufacturing processes. This cost effectiveness is because of its low weight and density. In total, 69 wrought aluminium grades were numerically simulated in the software and the values of each of the performance parameters were obtained. Because of having five different parameters based on which the best alloy had to be determined, a statistical approach of selecting the optimal alternative was required. Hence, with the help of the TOPSIS method which is a multi-criteria favoured approach that compares different samples by taking into account weights for each of those multiple criterias and normalises their individual scores with the help of which the most appropriate alternative is obtained.

This analysis would fetch us the best alternative for the selection of material to be used in the manufacturing of the crash boxes; however, there is a strong need of carrying out actual experimentation on those samples. This need comes from the fact that one cannot take into account all the actual imperfections that are existing in all the materials because of which all the material properties would deviate from the theoretically considered properties which are always based on some assumptions. Moreover, the simulation was carried out to simulate a quasi-static process (to have a reduced computational time) of compression, but in reality all the impact processes occur in a dynamic manner which becomes difficult and heavily time consuming to

simulate. Even though these limitations of carrying out numerical simulations are always encountered, the results of it can act as a primary basis for gathering an understanding of the material behavior under actual processes.

# **Contents**

1.	Introduction		
	1.1.	Crash-worthiness	1
	1.2.	Crash energy management	1
	1.3.	Relative positions of the structural members in a vehicle	3
	1.4.	Selection of material for manufacturing crash boxes	4
	1.5.	Designation system for Aluminium alloys	4
	1.6.	Tests carried out on crash boxes	8
	1.7.	Crashworthiness Performance Indicators	8
2.	Lite	rature review	10
3.	Obje	ectives problem statement and methodology	15
	3.1.	Objectives	15
	3.2. P	Problem statement and Methodology	16
4.	Num	nerical simulations	17
	4.1.	The need	17
	4.2.	Different numerical methods	17
	4.3.	Solving methodologies	18
	4.4.	Steps involved in the numerical analysis	19

5.	Results and discussion	30
6.	References	40

# **List of Figures**

Fig. No.	Name of Figure	Page No.
1	Ideal force displacement curve	
2	Actual force displacement curve	2
3	Illustration of structural members in a vehicle	3
4	Front View	15
5	Top View	16
6	Creating circular column/ crash box	20
7	True effective stress-strain curve	
8	Creating material properties	
9	Creating section property as thickness of the column	
10	Creating assembly	
11	Mesh size Vs. Mean force	23
12	Assigning element type to column	
13	Assigning element type to plates	
14	Final meshed assembly	25
15	Creating new step	26
16	Contact modelling between plates and column	27
17	Loading rate (velocity) distribution	27
18	Bottom plate boundary conditions	28
19	Applying load to the top plate (at reference point of the top plate)	28

20	Selecting reaction force (from bottom plate reference point) as one of the history output request	29
21	Simulation of the crushing behaviour of AA 2024 O under uniaxial quasi static compression	30
22	Deformation mode of AA 2024 O (Ring mode)	31
23	Force-displacement curve generated by operating on force and displacement curves (sample: AA 2618 T6)	31

# **List of Tables**

Table No.	Name of Table	Page No.
1	Aluminium alloy series with main alloying elements	
2	Basic temper designations	5
3	H temper subdivisions	6
4	T temper subdivision	6
5	T temper variations due to various heat treatment processes	7
6	True effective plastic strain and corresponding true effective stress values	20
7	Mesh size and respective mean forces	24
8	Results of simulations of all aluminium samples	32
9	Aluminium alloys for TOPSIS analysis	34
10	Normalised and weighted normalised values for each parameter	35
11	Deviation measurements and probability of selection for each sample	36
12	Deviation measurements and probability of selection for all the samples in the analysis	37

# **Symbols and Abbreviations**

 $\begin{aligned} F_{peak} & Peak \ Force \ (N) \\ F_{mean} & Mean \ Force \ (N) \end{aligned}$ 

CFE Crush Force Efficiency (%)
EA Energy Absorption Capacity (J)
SEA Specific Energy Absorption (J/kg)

m Mass of crash box (kg)

 $X_{1i}$  Crush Force Efficiency values corresponding to each sample

 $X_{2i}$  Specific Energy Absorption values corresponding to each sample

S+ Deviation from the best alternativeS- Deviation from the worst alternative

P Probability of selection

### Introduction

#### 1.1 Crash-worthiness

A vehicle's crashworthiness represents the ability of a vehicle structure and any of its components to absorb the crash energy during a collision such that the injury caused by external loads on the occupants are within the limits given by the motor vehicle safety standards.

By this definition of crashworthiness, one would want to have their vehicle to be crashworthy so that in the unfortunate event of a road accident or crash, the impact load on the occupants would be under the tolerable limit and the probability of severe injuries to the passengers would be minimal. According to ncrb 4,67,171 have died due to road accidents in 2019, the death toll may have reduced from 2018 but the number of road accidents per thousand vehicles remains the same [24]. The research on crashworthiness is henceforth aimed to minimise this damage. So in order to minimise the casualties, it is very important for the vehicles to be crashworthy. Crash worthy vehicles are designed in a way that the body structure undergoes progressive crush folds to absorb maximum kinetic energy of the crash and to protect the integrity of the passenger cabin. Crashworthiness evaluation is ascertained by a combination of tests and analytical methods based on numerical simulations. The crashworthiness of the vehicle and safety of the occupant are considered to be the two most important and challenging requirements in the vehicle design. In the current times, the vehicle structures are designed to control the crash deceleration pulse to fall below the limit of human tolerance besides maintaining the integrity of the occupant's compartment. A crash deceleration pulse with an early peak in time followed by a gradual decay is considered more beneficial for protection of a restrained occupant. This is because an early peak in deceleration reduces the occupant's velocity considerably and subsequently, even if the restrained occupant impacts with the vehicle's interior compartment, it happens at a much reduced velocity which will reduce the occupant's injury level. The design for crashworthiness provides an optimized vehicle structure that absorbs the crash energy in a short duration (milliseconds) by controlled vehicle deformations while maintaining adequate space so that the residual crash energy can be managed by the restraint systems.

#### 1.2 Crash energy management

The crash energy in the vehicular collision is to be absorbed as much as possible in a very short duration at the instant of impact by appropriate design of the vehicle structure so that the peak force transmitted to the vehicle is minimized. This in turn will reduce the level of deceleration pulse on the occupant. Various methods or designs have been explored and adopted for such requirements in energy absorption. The techniques adopted for quantification and control of crash energy is generally called crash energy management. Few parameters commonly used in quantifying the crash energy absorption of a vehicle. The peak force (Fpeak) is the maximum reaction force generated by the energy absorbing vehicular structure. This force should be allowed to fall below a threshold value irrespective of any possible crash. Ideally, this reactive

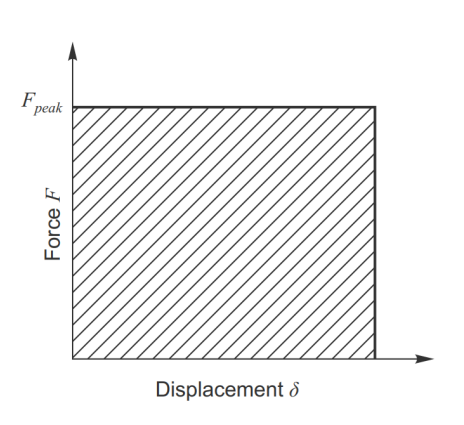
force has to be just below this threshold and remain almost constant during crash energy absorption. The crash kinetic energy EA absorbed by the vehicle structure is the work done by the crushing force F in inducing progressive deformation from an initial value  $\delta_i$  to a final  $\delta_f$  in the structure and is given by;

$$EA = \int_{\delta}^{\delta} Fd\delta. \quad (01)$$

It is the area under the curve between axial crush force F and deformation in structure.

Specific Energy Absorption (SEA) is the energy absorbed (Ec) by a unit mass m of the vehicle structure undergoing crash. Higher SEA means an efficient energy absorber and a lightweight crush member. Crush force efficiency is the ratio between the mean or the average crushing force  $F_{avg}$  and the peak crushing force  $F_{Peak}$  and is given as:CFE =  $F_{avg}$  /  $F_{Peak}$ . Ideally, CFE nearing 1 produces a constant force-deformation curve. Low CFE indicates a high peak force that causes higher deceleration levels in vehicles which may go beyond human tolerance and potentially harm the occupants during crashes.

Another way of assessing the crash energy absorption by a structural member of a vehicle is the energy absorbing characteristic curve which is between the crushing force and the deformation/displacement observed in the member:



 $F_{avg}$ Displacement  $\delta$ 

Fig. 1. Ideal force displacement curve

Fig. 2. Actual force displacement curve

Figure 1. shows the behaviour of an ideal energy absorbing structural component having the maximum area under the curve indicating that all the crash energy has been used up in deforming that member. But in reality, the curve closely resembles the one shown in figure 2. And it shows that the force experienced by the member is not constant throughout the impact process and because of it only some portion of the crash energy is absorbed to undergo deformation. [2]

# 1.3 Relative positions of the structural members in a vehicle

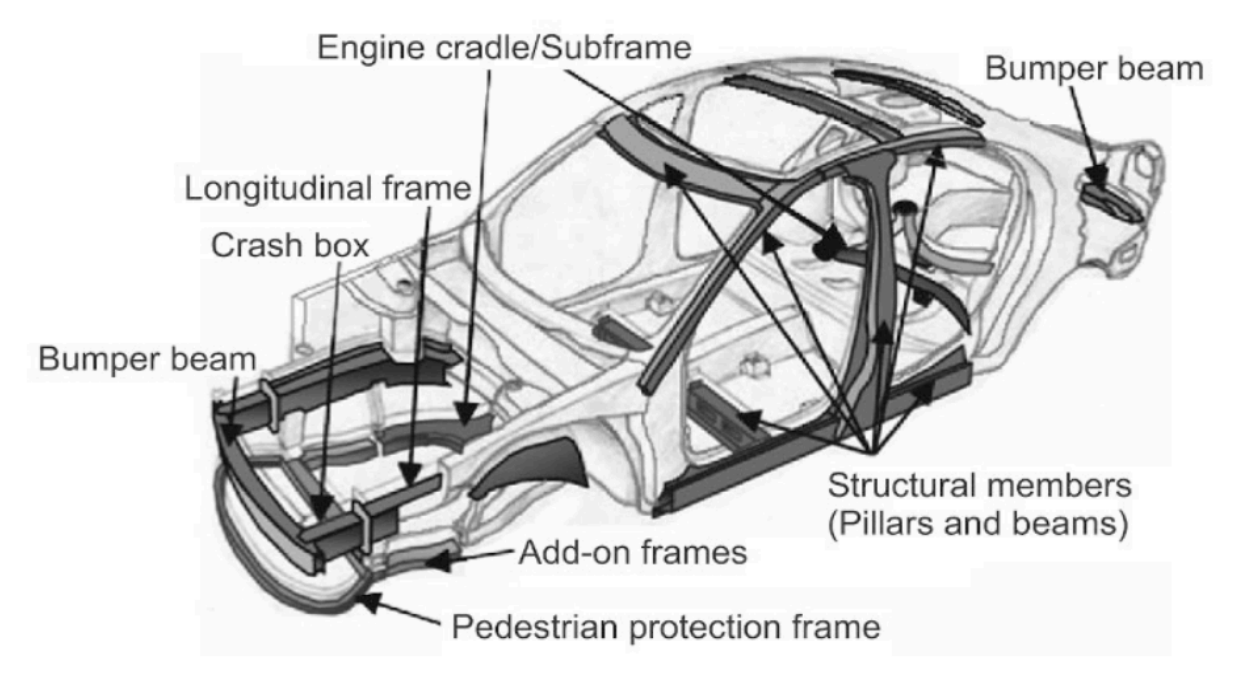


Fig 3. Illustration of structural members in a vehicle

#### Bumper beams

The bumper beams at front and rear of a vehicle minimize damage or injury by absorption of energy through elastic and eventually, plastic deformation during frontal and rear collisions. These members absorb energy through material deformation in a reasonably controllable manner and simultaneously protect occupants during a crash event by absorbing sufficient energy, without encroaching into the occupant compartment or by producing an undesirable level of deceleration. These are in direct contact with the crash boxes and because of that the crash energy is transmitted next to the crash boxes.

#### Crash boxes

Crash boxes act as energy absorbers and are a widely used component in many fields of transportation and have gained major importance in recent years in the domain of energy absorption in automobiles. They are structural members in the form of thin-walled metallic columns or tubes which deform drastically during a collision of the vehicle which results in dissipation of crash energy and reducing the damage to other structural components and the occupants. Other structural members (pillar and beams) are generally located on either side of the vehicle forming the main side-component during side impacts of the vehicle. The crash load of the moving deformable barrier or another colliding vehicle during side impacts is taken by these structural members at side of vehicle such as mid column, curved beams at bottom and top of side frames and the horizontal members at top and bottom hull of vehicle.

# 1.4 Selection of material for manufacturing crash boxes

Aluminium alloys are more preferred for making crashboxes than the magnesium and steel alloys due to its low weight and corrosion resistance, Aluminum alloy is a good alternative that can be recycled with much less required energy than that needed to produce primary aluminum. Magnesium alloys have lower specific heat than aluminum. The use of aluminum offers considerable potential to reduce the weight of an automobile body as compared to steel. Crashworthiness energy absorption is a key property of the material used for structural components or complete structures so-called "space frames". Aluminum alloys are highly strain rate sensitive which gives them advantages over carbon steel and magnesium alloys. This means that the faster the loading is applied the more the material will resist deformation.[1]

# 1.5 Designation system for Aluminium alloys

The Aluminum Association Wrought Alloy Designation System consists of four numerical digits, sometimes including alphabetic prefixes or suffixes. The below table shows the meaning of the first of the four digits in the alloy designation system. The alloy family is identified by that number and the associated main alloying ingredient(s).

Table 1. Aluminium alloy series with main alloying elements

Alloy number series	Main alloying element
1xxx	Mostly pure aluminum; no major alloying additions
2xxx	Copper
3xxx	Manganese
4xxx	Silicon
5xxx	Magnesium
6xxx	Magnesium and silicon
7xxx	Zinc
8xxx	Other elements (e.g., iron or tin)
9xxx	Unassigned

The second defines variations in the original basic alloy: that digit is always a zero (0) for the original composition, a one (1) for the first variation, a two (2) for the second variation, and so forth. Variations are typically defined by differences in one or more alloying elements of 0.15 to 0.50% or more.

The last 2 digits indicate the specific alloy within the series; there is no special significance to the values of those digits, nor are they necessarily used in sequence. However, for 1xxx series, those digits represent the two digits to the right of the decimal point in the minimum aluminum percentage specified for the designation when expressed upto 2 decimal places.

The temper designation system is based on sequences of basic treatments used to produce different tempers and their variations. This designation is always presented immediately following the alloy designation with a hyphen between the designation and the temper, for example 2014-T6. For basic temper designations, the first character in the temper designation is a capital letter indicating the general class of treatment. The designations are defined and described in the following table:

Table 2. Basic temper designations

Temper designated letters	definition
F (fabricated)	Applies to wrought or cast products made by shaping processes in which there is no special control over thermal conditions or strain-hardening processes employed to achieve specific properties. For wrought alloys there are no mechanical property limits associated with this temper.
O (annealed)	Products that are annealed to obtain the lower strength temper, usually to increase subsequent workability.
H (strain hardened)	Products that have their strength increased by strain hardening. The H is always followed by two or more digits.
W (solution heat treated)	Applies only to alloys that age spontaneously after solution heat treating. This designation is specific only when digits are used in combination with W to indicate the period of natural aging, for example, W 1/2 hr.
T (thermally treated other than F, O or H)	Products that are thermally treated, with or without supplementary strain hardening, to produce stable tempers. The T is always followed by one or more digits.

The H and the T temper designations are generally followed by two or more digits that make the subdivisions of those basic tempers. For the subdivision of the basic H temper, the first number(s) indicates the specific combination of basic operations as follows:

Table 3. H temper subdivisions

H1 (Strain hardened only)	Products that have been strain hardened to obtain a desired level of strength without a supplementary thermal treatment.
H2 (strain hardened and partially annealed)	Products that have been strain hardened more than the desired final amount, and their strength is reduced to the desired level by partial annealing.
H3 (strain hardened and stabilized)	Products that have been strain hardened and then stabilized either by a low temperature thermal treatment, or as a result of heat introduced during fabrication of the product. Stabilization usually improves ductility.
H4 (strain hardened and lacquered or painted)	Products that are strain hardened and that have been subjected to heat during subsequent painting or lacquering operations.

A digit following H1, H2, H3, or H4 indicates the degree of strain hardening as identified or indicated by the minimum value for tensile strength. For e.g. the hardest temper normally produced is indicated by adding the numeral 8 (i.e., HX8) and the numeral 9 is used to indicate tempers that exceed those of HX8 by 14 MPa or more.

For the subdivision of the basic T temper, the first number(s) indicates the specific combination of basic operations described below:

Table 4. T temper subdivision

T1	Products (a) that are not cold worked after cooling from an elevated temperature shaping process or (b) for which the effect of cold work in flattening or straightening may not be recognized in mechanical property limits
T2	Products (a) that are cold worked after cooling from an elevated temperature shaping process or (b) for which the effect of cold work in flattening or straightening may not be recognized in mechanical property limits
Т3	Products (a) that are cold worked to improve strength after solution heat treatment or (b) for which the effect of cold work in flattening or straightening is recognized in mechanical property limits
T4	<ul><li>(a) Not cold worked after solution heat treatment or</li><li>(b) The effect of cold work in flattening or straightening may not be recognized in mechanical property limits</li></ul>
T5	<ul><li>(a) Not cold worked after cooling from elevated temperature shaping process or</li><li>(b) The effect of cold work in flattening or straightening may not be recognized in mechanical property limits</li></ul>

Т6	<ul><li>(a) Not cold worked after solution heat treatment or</li><li>(b) The effect of cold work in flattening or straightening may not be recognized in mechanical property limits</li></ul>
Т7	Wrought products that are artificially aged after solution heat treating to increase their strength beyond the maximum value achievable.
Т8	<ul><li>(a) cold worked to improve strength or</li><li>(b) The effect of cold work in flattening and straightening is recognized in mechanical property limits</li></ul>
Т9	cold worked to improve strength
T10	<ul><li>(a) cold worked to improve strength or</li><li>(b) The effect of cold work in flattening or straightening is recognized in mechanical property limits</li></ul>

In all of the T-type temper definitions just described, solution heat treatment is achieved by Heating cast or wrought shaped products to a suitable temperature, holding them at that temperature long enough to allow constituents to enter into solid solution and then cooling them rapidly enough to hold the constituents in solution to take advantage of subsequent precipitation and the associated strengthening (i.e., precipitation hardening).

Additional digits are added to the T tempers to indicate a variation in treatment that significantly alters the product characteristics that are or would be obtained using the basic treatment. The specific additional digits shown in the below Table have been assigned for stress-relieved tempers of wrought products,

Table 5. T temper variations due to various heat treatment processes

Stress relieved by stretching	applications/ examples
TX51	Applies to plate and rolled or cold-finished rod or bar, die or ring forgings, and rolled rings when stretched the indicated amounts after solution heat treatment or after cooling from an elevated temperature shaping process.
TX510	Applies to extruded rod, bar, profiles (shapes), and tube and to drawn tube when stretched the indicated amounts after solution heat treatment or after cooling from an elevated temperature shaping process.
TX511	Applies to extruded rod, bar, profiles (shapes), and tube and to drawn tube when stretched the indicated amounts after solution heat treatment or after cooling from an elevated temperature shaping process.

Stress relieved by compressing	
TX52	Products that are stress relieved by compressing after solution heat treatment or cooling from an elevated temperature shaping process
Stress relieved by combined stretching and compressing	
TX54	Applies to die forgings that are stress relieved by restriking cold in the finish die.

#### 1.6 Tests carried out on crash boxes

For testing the crashboxes we could perform a quasi-static test or impact test in order to obtain a force displacement diagram. Quasi Static test could be performed and simulated, the displacement in the test undergoes slowly which enables us to observe each minute changes during the crash and we can get data on many mechanical properties of the material the procedural details differs for each material, but tests are usually conducted at room temperature at relatively slow loading rates (0.001-to-0.1 s-1) although various temperatures and loading rates may be required for the determination of material behavior under specific conditions, but quasi static is impractical to predict the the actual crashing using such a method, so in order to glean about the real life scenario we have to perform impact tests on the crashbox. Using impact tests are able to figure out the energy absorption of each material during the crash. We have simulated quasi static tests on the various aluminium alloys with the same dimensions due to limitations of the finance and the materials available. [2]

#### 1.7 Crashworthiness Performance Indicators

To measure and compare crashworthiness of crush tubes following performance indicators have been defined. These indicators can be obtained from the force displacement diagram, as shown in Fig. 2, of the crash box which can be obtained by carrying out quasi-static or impact loading analysis either numerically or experimentally.

# 1. Energy Absorption Capacity (EA):

Energy absorption capacity can be defined as an extent to which energy is absorbed by a crush box [13]. In other words, energy absorption is the work done by the external compressive load on the crush tube in the longitudinal direction up to given structural deformation [12]. For a particular structure, it can be calculated by measuring area under load-displacement plot of that structure. Mathematically, energy absorption can be defined as

$$EA = \int_{0}^{Smax} F(s) ds (2)$$

where,  $F_{(S)}$  is the instantaneous force defined in terms of displacement,  $S_{max}$  is the maximum allowable displacement of the tube.

# 2. Initial Peak Force (F<sub>peak</sub>):

Initial peak force ( $F_{peak}$ ) is that highest force which is required to generate first permanent deformation i.e. first fold in the tube [1]. In other words, initial peak force can be defined as the highest load that the tube can sustain before first failure [19].

# 3. Mean Force $(F_{mean})$ :

Mean force is defined as the energy absorbed by the tube when it is deformed by unit distance [16]. Mean force is that constant value of force if applied on the crush tube from start to end of the crushing process then the tube would have absorbed the same amount of energy as that of the actual case. Mathematically, it is a ratio of energy absorbed (EA) by tube in the crushing process to the maximum stroke length ( $S_{max}$ ). It indicates average crushing force all over the effective stroke [19].

$$Fmean = \frac{EA}{Smax}(3)$$

# 4. Specific Energy Absorption (SEA):

Energy absorbed per unit mass of the tube during the crushing process is defined as specific energy absorption (SEA) [19]. Mathematically, it is a ratio of energy absorbed by the tube (EA) to the mass of the tube (m).

$$SEA = \frac{EA}{m}(4)$$

# 5. Crush Force Efficiency (CFE):

A ratio of mean crushing force  $(F_{mean})$  to maximum force  $(F_{max})$  in the entire crushing action is termed as crush force efficiency (CFE).

$$CFE = \frac{Fmean}{Fmax}(5)$$

The crash box having higher value of  $F_{mean}$ , EA, SEA and CFE (closer to 1) but having lower value of Fpeak is said to be the better crash box as far as crashworthiness is concerned.

### 2. Literature Review

Using an INSTRON materials testing machine, Xiong Zhang & Hui Zhang [3] investigated the energy absorption properties of regular polygonal and rhombic columns under quasi-static axial compression. They studied the effect of central angle on deformation mode and mean crushing force of angle elements. Crush resistance of polygonal columns and angle elements under quasi-static and dynamic axial compression is also studied by them using numerical methods. The experimental results and the numerically predicted crushing force and deformation mode of the polygonal columns are considered to be in good agreement. Also, they have presented the deformation mechanism of energy absorption based on the experimental observations. Simple and multi-cell thin-walled aluminium tubes with triangular, circular, hexagonal, and octagonal parts were loaded quasi-statically in this study by A. Alavi Nia & M. Paraspour [4]. The results of the experiments were then compared to numerical simulations. The findings revealed that multi-cell sections have a higher energy absorption ability than simple sections. They found that in a multi-cell configuration, hexagonal and octagonal sections have absorbed the most energy per unit of mass. Z. Fan et al. [5] studied four types of geometries for thin-walled tubes experimentally. They are hexagon, octagon, 12-sided and 16-sided star, respectively. Experimental data are then compared with those predicted from FE simulations using ABAQUS. It is shown that the experimental and the corresponding numerical results are in agreement with each other. The rise in inward corners shows a positive change in energy absorption, but only to a certain degree. When the D/t ratio is less than 50, the 12-sided star shape has the best energy absorption capability, where D is the notional diameter and t is the thickness. In comparison to the other shapes tested, the 16-sided star performed poorly. To increase the energy absorption potential, Shing Zhao et al. [6] proposed a novel origami-ending tube. As compared to the conventional tube, the origami-ending tube could deform in the desirable diamond mode with a 46 percent reduction in Fmax and a 99 percent increase in Fm. In terms of energy absorption capacity and manufacturing, the origami-ending tube outperforms the origami crash box. Ali Alavi Nia &Jamal Haddad Hamedani [7] examine the deformations and energy absorption capacity of thin-walled tubes with various section shapes (circular, square, rectangular, hexagonal, triangular, pyramidal, and conical) both experimentally and numerically. The tubes are subjected to axial quasi-static loading and have the same volume, height, average section area, thickness, and material. The simulation results agree well with the experimental data, indicating that the section geometry has a significant impact on energy absorption. Of all the investigated sections, the circular tube has the highest energy absorption ability and the highest average force. Due to their uniform load-displacement curves and therefore less difference between the maximum and average forces, pyramidal and conical tubes are recommended in impact events where the maximum force is concerned. Jie Song et al. [8] introduced Patterned windows to the thin-walled square tubes to reduce the weight while maintaining the mechanical property of the original tube. Under axial compression, they investigated the topological pattern design. Experimental results show that these windowed tubes outperform conventional tubes in terms of crushing performance, with a maximum reduction in initial peak load of 63 percent and

a maximum increase in specific energy absorption of 54 percent. The effect of window size on tube collapse characteristics is investigated in a parametric study using finite element analysis. There are three types of collapse modes: symmetric, extensional, and diamond. Tubes that collapse in the diamond mode have lower energy absorption and SEA, while those that collapse in the symmetric or extensional mode have higher SEA. To better understand the crashworthiness of aluminium alloy joints produced by FSW(Friction Stir Welding), A. K. Lakshminarayanan & Cyril Joseph Daniel [9] conducted this investigation to fabricate a frontal member top hat section with a base member welded using three separate friction stir welding process variants in order to better understand the crashworthiness of aluminum alloy joints developed by FSW. The crashworthiness of the fabricated joints was investigated by applying quasi-static loading to them, and the results were published. They investigated the crashworthiness of the fabricated joints by applying quasi-static loading to them, and the results were published. The findings of the experiments are compared to those of the numerical simulation. F Tarlochan et al. [10] described the design of a thin wall structure subject to dynamic compression in both axial and oblique directions using a computationally assisted design method. To find the cross-section that meets the performance requirements, several different cross-sectional shapes of thin-walled structures subjected to direct and oblique loads were compared first. The decision was made using a multi-criteria decision-making mechanism (MCDM). The absorbed crash energy, crush force strength, ease of manufacture, and cost are the performance parameters used. Following the selection of the cross-section, the design was improved for better crash efficiency by looking into the impact of foam filling, increasing the wall thickness, and adding a trigger mechanism. The new design was able to increase crash efficiency by an average of 10%, which was a very promising result of the design process. For the quadruple-cell origami-patterned tubes, theoretical analyses based on simplified buckling models and a theoretical solution for the mean crushing force were derived by Kai Yang [11]. With balanced initial peak force, specific energy absorption, and crushing force fluctuation, a series of optimal designs were obtained. According to the findings, origami-patterned and origami-triggered quadruple-cell tubes can maintain relatively high specific energy absorption (SEA) as compared to conventional quadruple-cell square tubes, with origami-patterned quintuple-cell tubes having the highest values. Selective laser melting (SLM) is a well-established process for fabricating structures that can withstand static loads and small strains. Zhe Yang et al. [12] have used the SLM method to build a 316L stainless steel thin-walled circular tube with preset internal circumferential rectangular groove defects. Split and MTS compression Hopkinson Pressure Bar tests are used to assess the material behaviour of SLM printed 316L stainless steel, and the results are used to match Johnson-Cook constitutive model parameters. The drop hammer test and finite element analysis was used to investigate the crushing behaviour of the SLM printed tube both experimentally and numerically. The buckling stage and the splitting stage are the two stages of the tube crushing process, as shown by the results. Internal grooves control the initial buckling position as well as the fracture position during the buckling stage. In one simple structure, the double buckling-splitting crushing mode

offers a new energy absorption approach for engineering applications. Kai Yang et al. [13] proposed a novel type of tubular structure in which pre-designed ellipsoidal dimples were inserted into circular tubes. Finite element modelling was used to investigate the impact of various dimple design parameters on mechanical properties, which was then experimentally validated using quasi-static experiments on 3D printed brass tubes. The findings showed that properly constructed dimpled tubes had a lower initial peak force and surprisingly less fluctuation in crushing force than circular tubes, without reducing the mean crushing force significantly. Three new energy absorbers based on uniform grooved tube (UGT) are proposed by Ru-yang Yao et al. [14] depth gradient grooved tube (D-GGT), thickness gradient grooved tube (T-GGT), and coupling gradient grooved tube (C-GGT). They propose a theoretical model that considers both depth and thickness gradients, as well as an efficient numerical model based on the axisymmetric assumption. Quasi-static compression experiments are carried out to verify the theoretical and numerical models. The results indicate that under axial buckling, the deformation of gradient grooved tubes (GGTs) can be divided into two modes: random asymptotic buckling (RAB) and sequential asymptotic buckling (SAB) (SAB). When compared to UGT, the D-GGT has a slight improvement in axial energy performance, despite the fact that the sum of the depth of thin-walled sections remains constant; for T-GGT, a force-displacement curve with an upward trend and an apparent improvement in energy absorption are observed; and, when C-GGT is subjected to axial loading, the energy absorption characteristics of D-GGT and T-GGT will occur simultaneously. By replacing the inner tube with half-cylindrical shells acting as stiffeners around the circumference of the external tube, Manmohan Dass Goel [15] attempted to improve the energy absorption of thin concentric cylindrical tubes. Under impact loading, the tubes were simulated and their deformation and energy absorption were investigated in terms of bottoming-out and energy absorption effectiveness factor. For the purpose of comparison, the total mass of the stiffened and double tubes is kept the same. The energy absorption capacity of the double tube is 1.71 times that of the single tube, and the stiffened tube configuration is 1.91 times that of the single tube. Furthermore, as compared to the single tube configuration, the energy absorption effectiveness factor is 1.69 times higher for double tubes and 1.89 times higher for stiffened tubes. The crushing mechanisms of two types of thin-walled structures, holed tube and grooved tube, were investigated using analytical, numerical, and experimental methods by Saharnaz Montazeri et al. [16]. By inserting grooves and holes at fixed intervals along the tube, plastic deformation was occurring. Crushing performance of grooved and holed models were analysed using finite element simulation and then tested with experiment for this purpose. First, analytically, numerically, and experimentally, the crushing performance, load-displacement curve, energy absorption, mean crushing load, and Mass specific energy (SEA) of grooved and holed thin-walled mild steel tubes were compared. Second, the crushing mechanics of holed and grooved tubes were studied and then, load-displacement curves of holed steel tube and grooved steel were studied, followed by the load-displacement curves of holed thin-walled tubes made of mild steel and aluminum. According to the findings, the holed thin-walled aluminum tube has the maximum crushing performance, SEE, and energy absorption. The structural response and crashworthiness performance of a hexagonal thin-walled grooved tube subjected to axial and oblique impact loading conditions were investigated numerically by Chukwuemeke William Isaac and Oluleke Oluwole [17]. For both hexagonal and circular tubes subjected to high dynamic impact loading conditions, an analytical formulation that estimates the mean crushing force and total energy absorption is obtained first. The approximate solutions of the finite element model are compared and checked using the analytical model's solutions. Muhammad Kamran et al. [18] introduced a new concept involving a bi-tubular tube with an outer straight cylindrical tube and an inner tube with a semi-apical angle, with dynamic axial loading monitored. Four straight stiffeners connect the outer and inner tubes. The sensitivity of energy absorption is investigated by varying the semi-apical angle of the inner tube, known as  $\beta$ , from zero to two degrees. The sensitivity of  $\beta$  is also examined using an analytical approach. To demonstrate the effectiveness of the proposed configurations, the results are compared to experimental and theoretical results. Wangyu Liu et al. [19] focused on the axial dynamic performances of the thin wall tubes with star-shaped cross-sections (S-tube). To begin, impact tests on Aluminum S-tube samples are carried out to ensure that the numerical simulation is accurate. Then, based on simulations with tubes of various dimensions, a mode classification chart is given. The slenderness of the tube is found to play an important role in the deformation mode. Wangyu Liu et al. [20] examined the crashworthiness of thin-walled tapered tubes with a star-shaped cross-section under oblique impact. To begin, compressive tests are used to validate the finite element model. The tapered star-shaped tube is then impacted at five different loading angles, with impact responses assessed using parameters including peak force (Fmax) and specific energy absorption (SEA). Abbas Rahi [21] looked into the effect of geometry on the energy absorption of aluminium tubes with various cross-sections, as well as the ability of combined bi-tubular tubes to absorb more energy when subjected to axial crushing. Aluminum tubes with circular and square cross-sections were prepared for the experimental portion, and then quasi-static tests with static loading rates were performed, giving load-deflection diagrams for each test. To simulate the collapse process, a numerical model based on finite element analysis is proposed, taking into account nonlinear responses due to material behaviour, contact, and large deformation. Mohd. Revaz Ur Rahim et al. [22] conducted a crashworthiness study of thin-walled corrugated tubes made of structural steel and compared their findings to the energy absorption values observed during aluminium alloy energy absorption tests. Tower cranes, roof shades, purlins, columns, and chimneys are all examples of thin-walled cylindrical tubes in engineering. As a result, it is necessary to examine how corrugated thin-walled structural steel tubes work in energy absorption tests. To improve the crashworthiness performance of bi-tubular profiles, Quirino Estrada et al. [23] evaluated the effect of cross-section, bi-tubular clearance and holes as crush initiators using finite element simulations. A Johnson-Cook (J-C) failure model was used to model harm in aluminum 6063-T5. Bi-tubular arrangements based on polygonal and circular cross-sections were tested using quasi-static compression loads during the cross-section study. According to the findings, circular shapes outperformed square base structures in terms of crashworthiness or crush force efficiency (CFE) by up to 12.28 percent. When the

non-dimensionalized clearance between profiles is increased from  $\lambda$  = 20 to  $\lambda$  = 40, CFE improves by 10.72 percent. Drilling holes in various positions in both the inner and outer profiles was used to test the effect of holes on crashworthiness performance. The results show that using holes improved the crush force efficiency and energy absorption (Ea) capacity even more than just using clearance.

# 3. Problem Statement and Methodology

To reduce the overall weight of an automobile and thereby to minimize the emission of hazardous gases from the automobile and to increase the fuel efficiency of the vehicle, steel alloys are getting replaced by aluminium alloys in automobile industries. Various aluminium alloys, listed in Chapter 2, are used to manufacture different structural members that are used in automobiles, as shown in Fig. 3. Crash boxes, also known as thin walled collapsible energy absorbers, are nowadays fabricated from various aluminium alloys instead of steel alloys because of above mentioned reasons. Researchers have studied crash boxes made up from various aluminium alloys for their crashworthiness properties by carrying out axial and oblique quasi-static as well as impact testing, experimentally and numerically. Moreover, a number of attempts have been made to enhance the crashworthiness performance of crash box. Literature based on the crash box given in Chapter 2 above, shows that crash boxes manufactured from various aluminium alloys collapse in different ways and have different crashworthiness properties. Crush response of aluminium crash boxes have been examined by various researchers but a collective study of all the aluminium alloys stating the best suited aluminum alloy for crash box is unavailable, to the best of author's knowledge. Hence to determine which aluminium allov and its temper is best suited for the crash box, this project is undertaken.

# 3.1 Objectives:

Following are the objectives of the current project,

- 1) To carry out quasi-static axial compression of crash boxes made up of different aluminium alloys numerically by using commercially available FE software ABAQUS/Explicit.
- 2) To determine the aluminum alloy having better crashworthiness performance by using TOPSIS a multi-criteria decision making method.

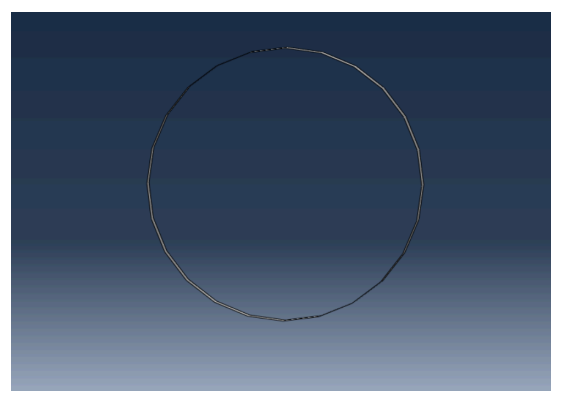


Fig 4. Front view

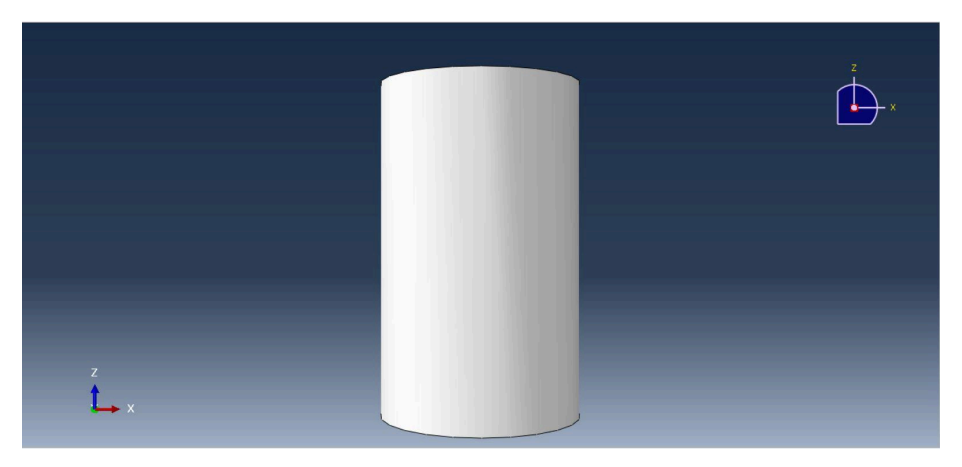


Fig 5. Top View

# 3.2 Problem statement and Methodology:

To choose the material for the crash box, a cylindrical tube which is commonly employed as a crash box in the past literature, is used in this project. This cylindrical tube, shown in Fig. 4 and 5, has a mean diameter (D) of 60 mm, thickness (t) of 2 mm and length (L) of 100 mm. These overall dimensions of the crash box are kept constant throughout the project while its material properties like elastic, plastic stress-strain properties have been changed as per the aluminium alloy used. Quasi-static axial compression of such cylindrical tubes made up of different aluminium alloys needs to be carried out to find out their crashworthiness properties like peak force (F<sub>peak</sub>), mean force (F<sub>mean</sub>), crush force efficiency (CFE), energy absorbed (EA), specific energy absorbed (SEA) and mode of collapse as well. It was decided to carry out numerical simulations of this quasi-static compression of crash boxes by using commercially available finite element package ABAQUS/Explicit in this entire project. A representative numerical simulation is explained in detail in step by step manner in Chapter 4. The aluminium alloy giving higher CFE and higher SEA will be treated as beneficial aluminium alloy for the crash box. After getting crush responses of tubes made of different aluminium alloys, TOPSIS - one of the frequently used multicriteria decision making techniques, is employed to select the aluminium alloy having beneficial crashworthiness properties. A sample calculation for TOPSIS is shown in Chapter 5.

# 4. Numerical simulations

#### 4.1 The need

Numerical simulation methods have proven to be most effective and reliable in the field of engineering which yield approximate but accurate results for most of the real life complicated engineering problems. These simulation methodologies require very low cost and setup time as compared to higher costs involved in actual testing of materials or prototype designs such as material cost and equipment setup-up costs. However, these numerical simulations cannot completely replace the actual experimentation process as these simulations are carried out by carrying some few assumptions that may not be true in practical situations and hence the practice of verifying the simulation results with the actual experimental results is generally preferred. Many engineering problems are often spread across different domains of studies and research such as aerodynamics, thermodynamics, fluid dynamics, impact mechanics, etc. and in order to approach those problems effectively, few numerical methods are often preferred depending on the extent to which the solution is needed.

#### 4.2 Different numerical methods

Finite element method (FEM)

It is the most popular method, which uses the principle of discretizing a continuous object into a finite number of elements and hence reducing the degree of freedom of the whole object. These elements are joined at nodes, on which all the calculations are done. For the crashworthiness analysis of the crash tubes, FEM or FDM are the most prefered numerical methods.

#### Finite difference method (FDM)

This method shares many common things with FEM. It is described as a way to solve the differential equation, as it uses Taylor's series to convert a differential equation into an algebraic equation and the higher order terms are often neglected.

### Boundary element method (BEM)

This method is often prefered to solve acoustics or noise, vibration or harness (NVH) problems. Like the FEM, it also uses nodes and elements but only takes into account the boundary of the domain. So if the problem is of a volume domain or an area domain then only the outer surfaces and the periphery are considered respectively. This way it reduces the dimensionality of the problem by one degree and which enables it to solve the problem faster.

#### Finite volume method (FVM)

All computational fluid dynamics (CFD) softwares are based on this method which considers a finite volume which is similar to an element in FEM and is based on the Navier-stokes equation. The varying properties at nodes are pressure, velocity, area, mass, etc [2].

#### 4.3 Solving methodologies

Given a problem in the structural crashworthiness field, the main objective is to obtain some of the most important quantities like, plastic stresses, contact forces, energies such as kinetic, potential and overall energy absorption characteristics. These quantities are strictly dependent on basic physical quantities like displacements, velocity and acceleration given the initial conditions on displacement and velocity with respect to time. A dynamic system is defined by its equations of motion (or equilibrium equations for transient dynamics), which for a crashworthiness analysis would be as follows:

$$\{M\}\{\frac{d^2u}{dt}\} + \{C\}\{\frac{du}{dt}\} + \{K\}\{u\} = \{F_{ext}(t)\}$$
 (02)

(inertial force + damping force + stiffness force = External force)

Where u is the general displacement vector, M is the mass matrix, C is the damping matrix, K is the stiffness matrix and  $F_{ext}(t)$  is the external load vector [2]. There are two methods of solving these equations using finite element method (FEM) which are the implicit and explicit methods. Here, FEM is used only for spatial discretization and the Finite difference method (FDM) for temporal discretization. The total response of the system is divided into smaller intervals called time steps or increments and then the equilibrium equations are solved at  $t+\Delta t$  based on the knowledge of the variables at time t.

#### **Explicit Integration scheme**

In the Explicit method, the information at time step n+1 can be obtained in terms of the previous steps and there is no dependence on the current time step. The equations of motion are written as

$$\{M\}\{\frac{d^{2}u}{dt}\}_{n} + \{C\}\{\frac{du}{dt}\}_{n} + \{K\}\{u\}_{n} = \{F_{ext}(t)\}_{n}$$
 (03)

Where n is the time level index. The mass matrix can be diagonal/ fully filled while the damping matrix is to be made diagonal by suitable approximations. With the help of the central difference operator (second order) and by employing the Von-Neumann stability conditions it is found that the time t, for the whole process should be small enough such that the information doesn't propagate across more than one element per time step [2].

Courant No. = 
$$\frac{C\Delta t}{\Delta x} \le 1$$
 (04)

Where  $\Delta x$  is the length of the element and C is the elastic wave speed.

As the time step becomes very small (e.g in the order of 1e-0.6 for 5mm mesh size) which happens in the case of very high frequency loads (e.g. crash problem), explicit integration schemes become very efficient and economical to use. It also provides high computational speed as there is no matrix inversion involved.

#### Implicit Integration scheme

In implicit method, equilibrium is achieved at each time using an iterative procedure, and so the accuracy of the method depends on the procedure and the convergence tolerances. Common algorithm used is the  $\beta$ -Newmark time integration which uses Taylor series discretization in the given manner;

$$\{u\}_{n+1} = \{u\}_n + \Delta t \{\frac{du}{dt}\}_n + \Delta t \left[(\frac{1}{2} - \beta)\{\frac{d^2u}{dt}\}_n + \beta\{\frac{d^2u}{dt}\}_{n+1}\right]$$
(05)

Where  $\beta$  is a parameter of the system

A tolerance is specified for u in various norms so as to ensure a correct convergence. Each increment consists of a minimum of one iteration, thus the computational cost is proportional to the model size.

Implicit schemes show faster speed than explicit for small to moderate problems only whereas explicit ones become much faster towards high end applications. Implicit schemes are efficient for structural dynamics problems with low to moderate frequency content and since these are of longer duration, larger timesteps can be considered. All static solution methods use implicit procedures [2].

### 4.4 Steps involved in the numerical analysis

The numerical analysis was carried out in the ABAQUS CAE software by Dassault systems. In order to approach the problem, quasi-static analysis was carried out and the results were obtained by using the explicit methodology with the help of ABAQUS/ Explicit Solver. The mesh sensitivity analysis and the results validation are based on the literature survey done in the research work of Alkhatib, S. E., Matar, M. S., Tarlochan, F., Laban, O., Mohamed, A. S., & Alqwasmi, N. on the "Deformation modes and crashworthiness energy absorption of sinusoidally corrugated tubes manufactured by direct metal laser sintering".

### 4.4.1 Geometry and parts creation

For the purpose of this project, a circular column is modelled with 62 mm as its outer cross sectional diameter, 2 mm as thickness and 100 mm length. This column is modelled as a 3D shell extruded model and has been given the section property of thickness of 1mm. While creating the cross section of the column the diameter was taken as 60 mm (mean diameter) so as to

accompany the thickness of the tube. The top and bottom plates are modelled as 3D discrete rigid shell planar bodies with square cross section dimensions of 70 x 70 mm each.

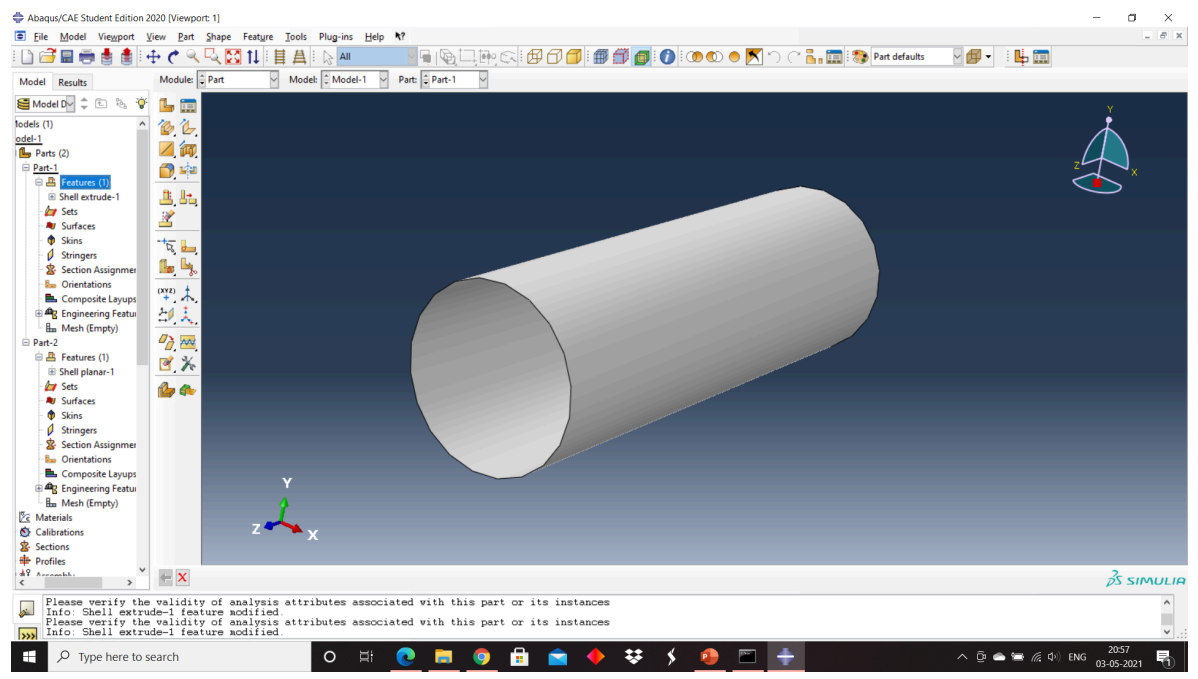


Fig 6. Creating circular column/ crash box

# 4.4.2 Material property definition

Basic mechanical properties like density and young's modulus were specified under the "property" module and in the material manager. As an example; density was given as 2.67 E-9 tonne/mm<sup>3</sup>, the modulus of elasticity as 56 E3 MPa and the poisson's ratio as 0.3. In order to introduce plastic behavior, the true effective stress and true effective plastic strain curves were defined by entering the respective values of stresses and strains under the plastic material behaviour section for all the aluminium samples taken for this analysis. An example of this plastic behaviour is shown in the following true effective stress-strain curve represented in tabular format.

Table 6. True effective plastic strain and corresponding true effective stress values

True effective plastic strain	True effective stress (MPa)
0.000	106.103
0.013	178.113
0.029	202.100

0.045	212.786
0.060	219.710
0.076	224.792
0.091	228.327
0.091	228.489

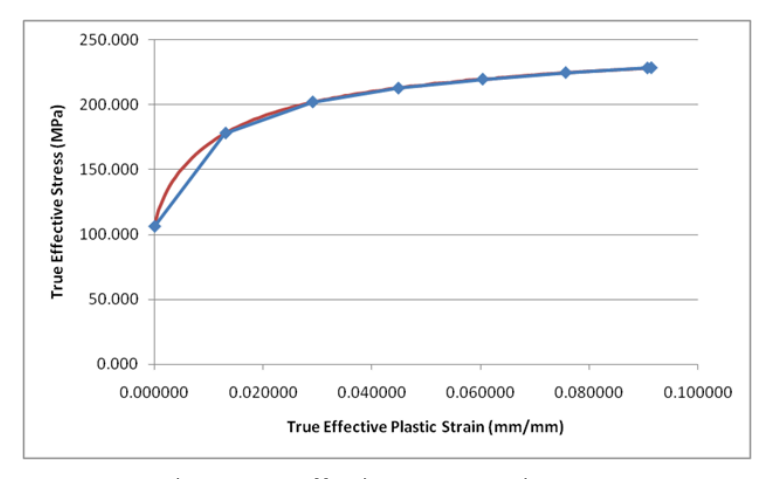


Fig 7. True effective stress-strain curve

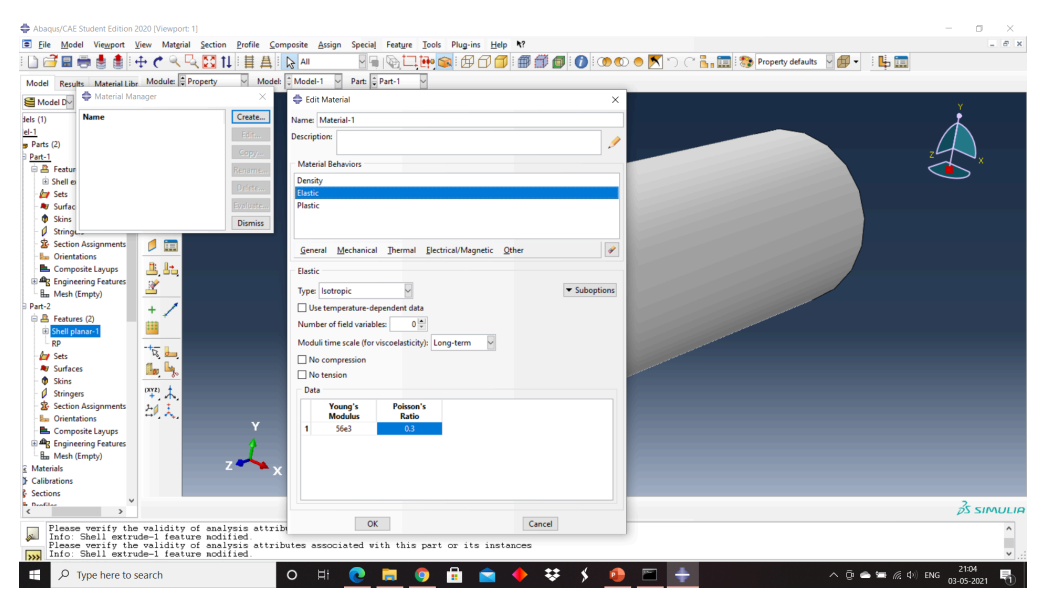


Fig 8. Creating material properties

The plates were already modelled as rigid bodies in order to perform quasi-static analysis of the crash tube and hence require no material property definition.

### 4.4.3 Section property definition

The column can approximately be seen as a 2D surface as its thickness is very small in comparison to its other dimensions and so the section property is defined to incorporate that point. The thickness of the circular column is specified by considering the cross sectional surface of the column as the mid-surface.

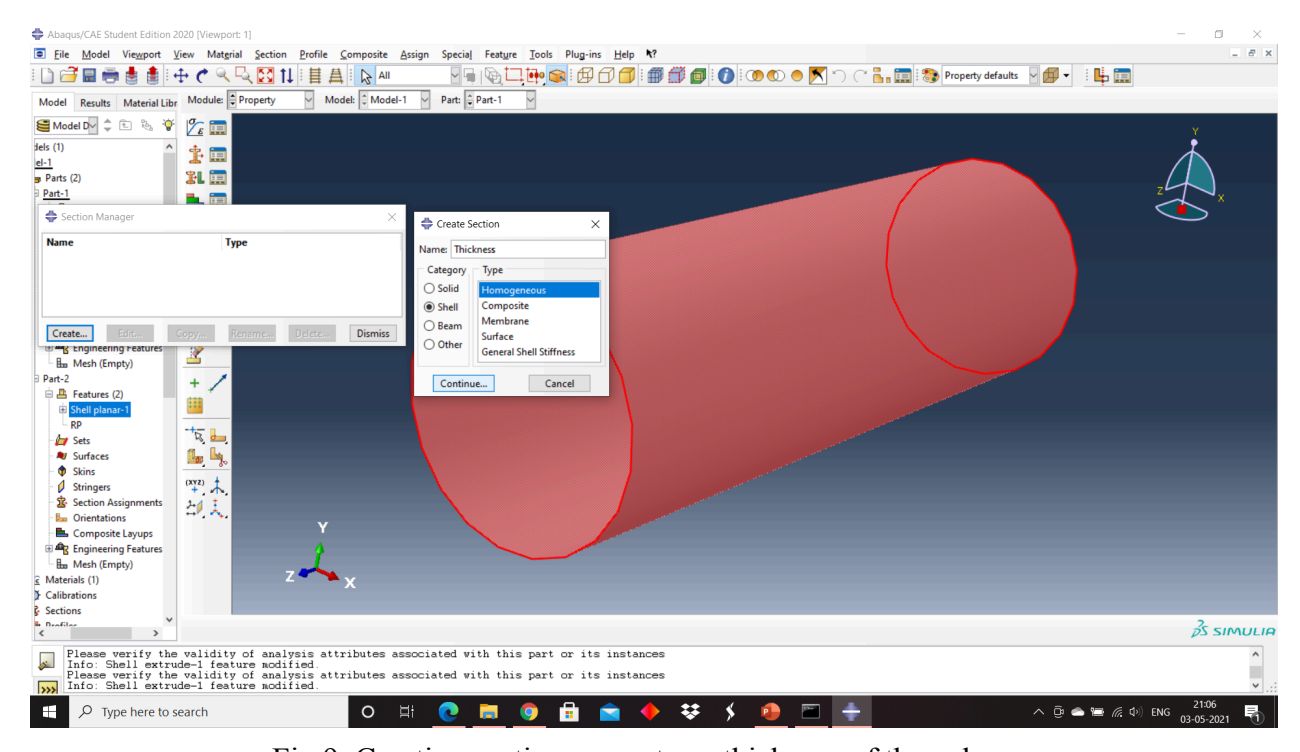


Fig 9. Creating section property as thickness of the column

### 4.4.4 Assembly creation

The method used for assembly as quoted in the literature is to produce a real life accident situation. The lower plate was attached to the bottom side of the column and the top plate was attached to the top side of the column via some specified interaction algorithms.

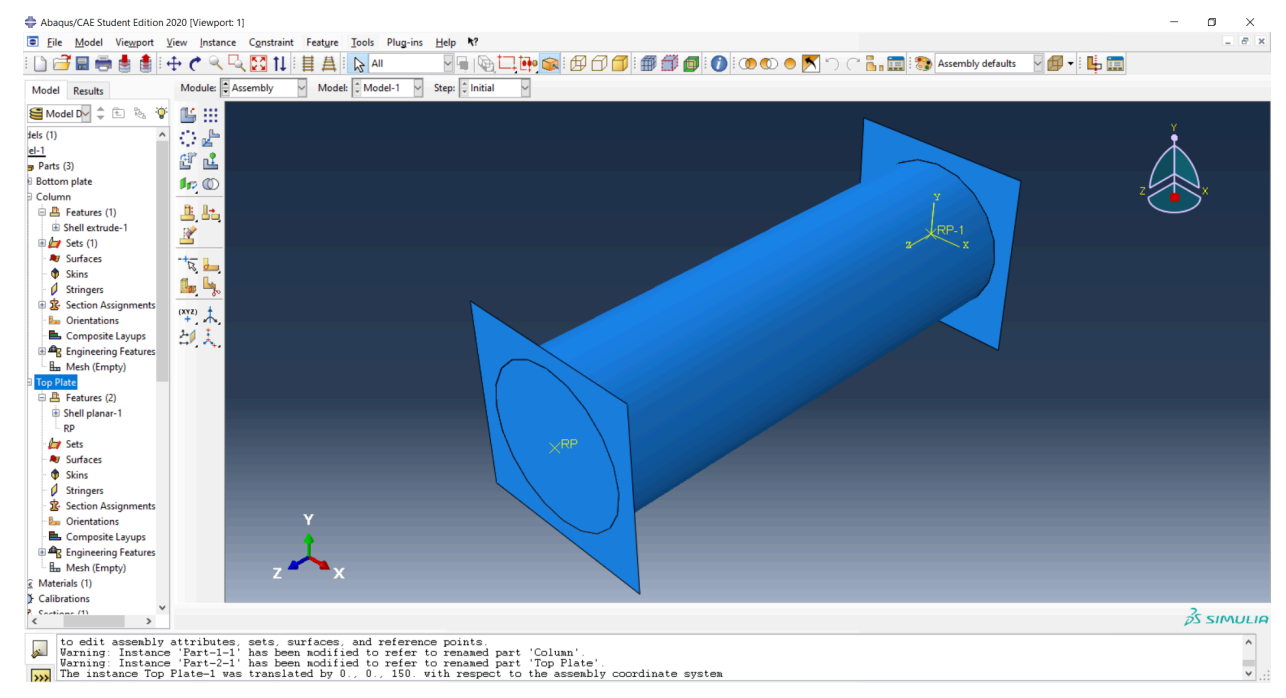


Fig 10. Creating assembly

# 4.4.5 Meshing

Different types of elements were used for the column and the plates. For the column, S4R element type is chosen which is a 4 noded linear element that offers hourglass control with reduced integration. Plates were assigned a 4 node 3D bilinear quadrilateral element. The global mesh size as inferred from the mesh sensitivity analysis from the literature was set as 2 mm for the column and for the plates it was taken as 6 mm in order to have reduced computational time. The following table shows the mesh sensitivity analysis from the literature.

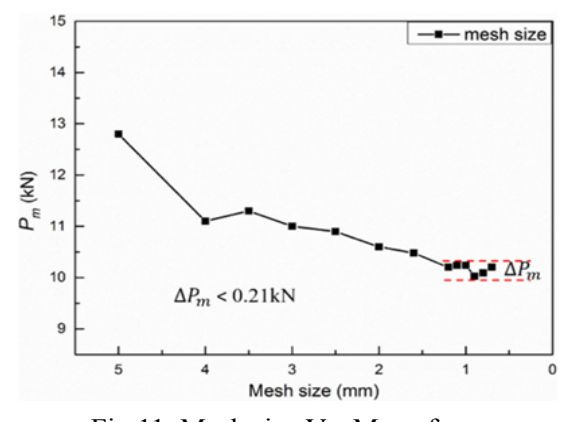


Fig 11. Mesh size Vs. Mean force

Table 7. Mesh size and respective mean forces

Mesh Size (mm)	Mean Force (kN)
5	13
4	11
3	10.8
2	10.5
1	10.3

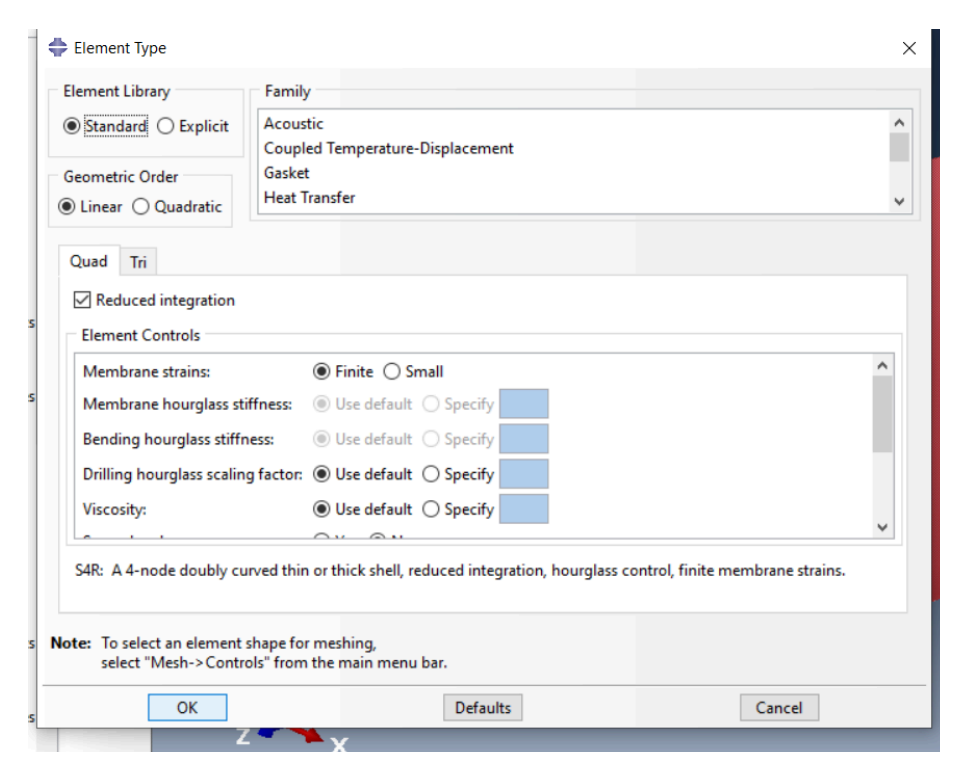


Fig 12. Assigning element type to column

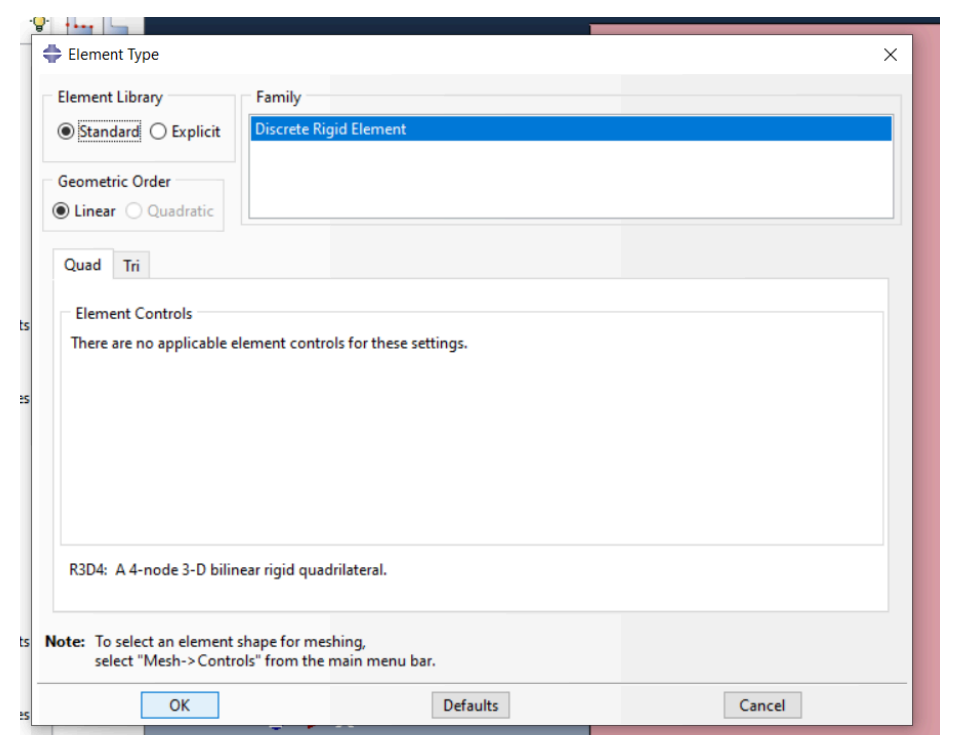


Fig 13. Assigning element type to plates

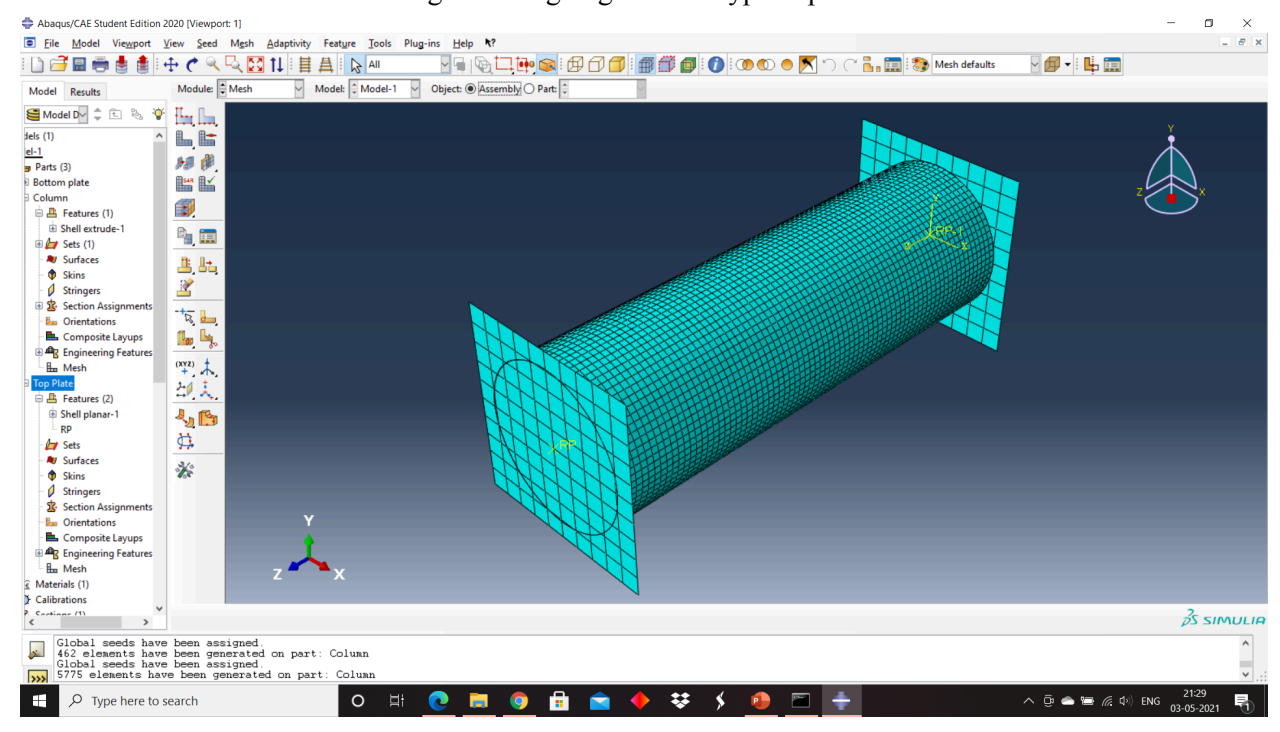


Fig 14. Final meshed assembly

# 4.4.6 Steps creation

An initial step was chosen in order to apply the boundary conditions and the loads and another step was created with a procedural type of "dynamic, explicit" to account for the loading and the deformation process of the column. This step was given a time period of 0.12 secs in order to satisfy the condition that the loading rate would be such that the total kinetic energy of the system falls under the quasi-static requirement of the problem (i.e. less than 5% of the total internal energy of the system) when the deformation is allowed upto 80% of the total length of the column/ tube.

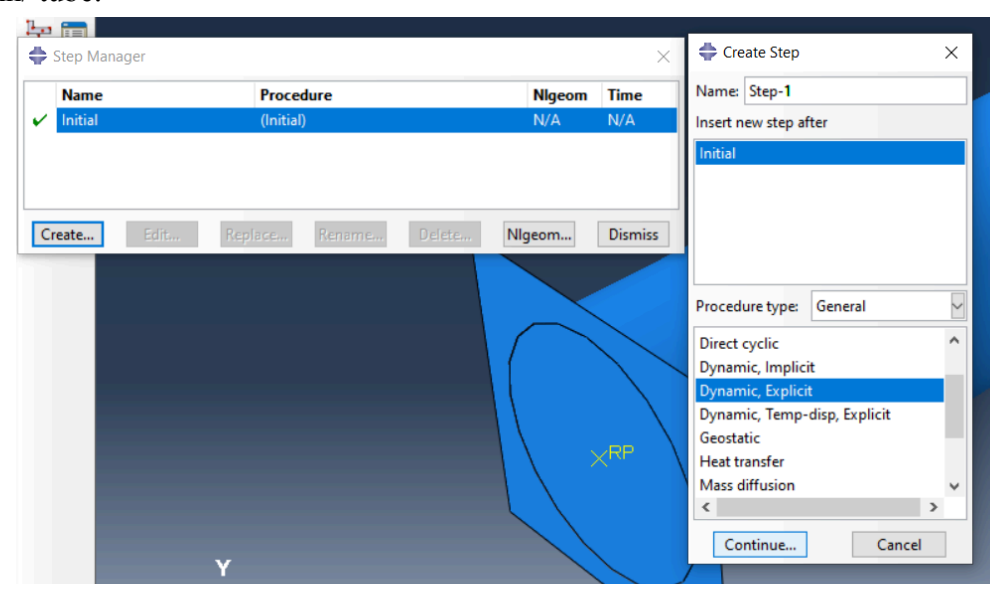


Fig 15. Creating new step

### 4.4.7 Contact modelling

A contact is a non permanent, uni-directional and friction based surface interaction between the modelled parts. This was modelled in order to prevent the inter-penetration of the parts into each other. In the current numerical simulation, general contact algorithm was used to model the interaction between plates and tube and the tube with itself in order to prevent self penetration of the tube. The friction coefficient as required by the penalty based friction formulation, was set to 0.2.

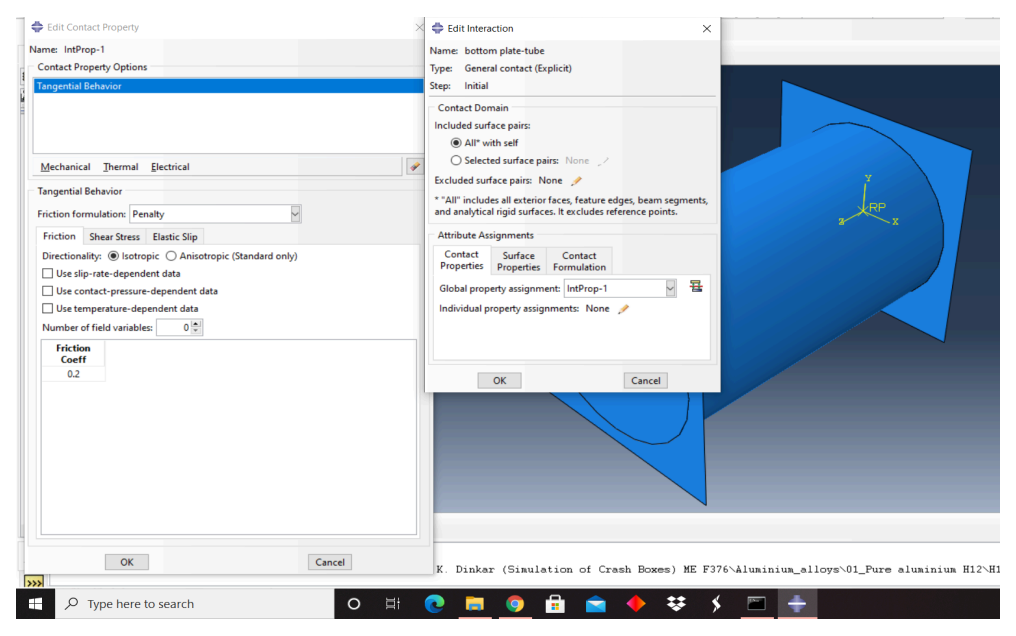


Fig 16. Contact modelling between plates and column

# 4.4.8 Boundary conditions and load specifications

In order to apply the boundary conditions on the plates, a reference point is created on both the plates. The bottom plate was given encastre boundary condition which constrains it in all directions and assigns all the degrees of freedom as zero. The top plate was given a displacement/ rotation type boundary condition in which only the vertical (Y direction) motion was unrestricted and rest, other degrees of freedom were fixed. In order to simulate a quasi-static testing, the loading rate was kept less than 5% of the wave propagation speed in the column. Loading rate was set to 1000 mm/sec and was assigned to the top plate. A velocity boundary condition was applied to simulate the loading rate in a non uniform manner as shown:

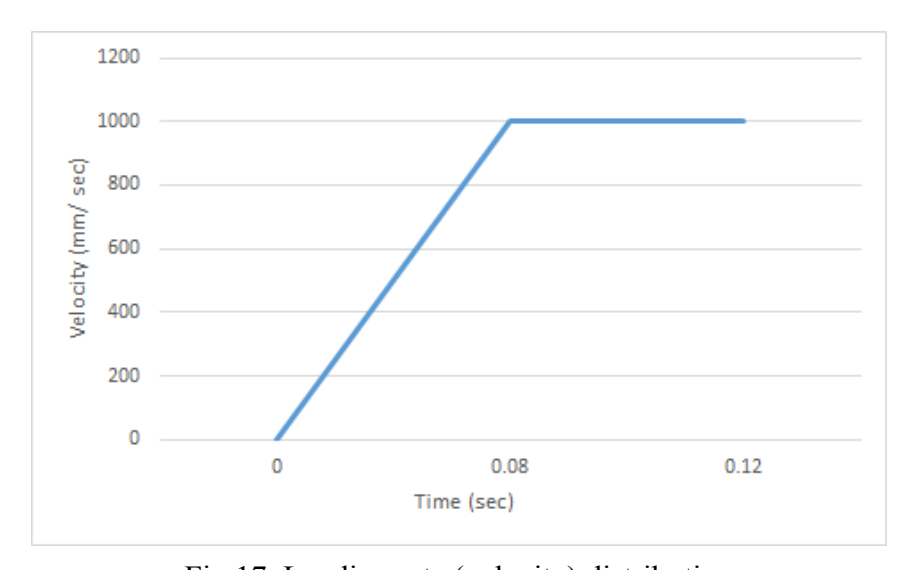


Fig 17. Loading rate (velocity) distribution

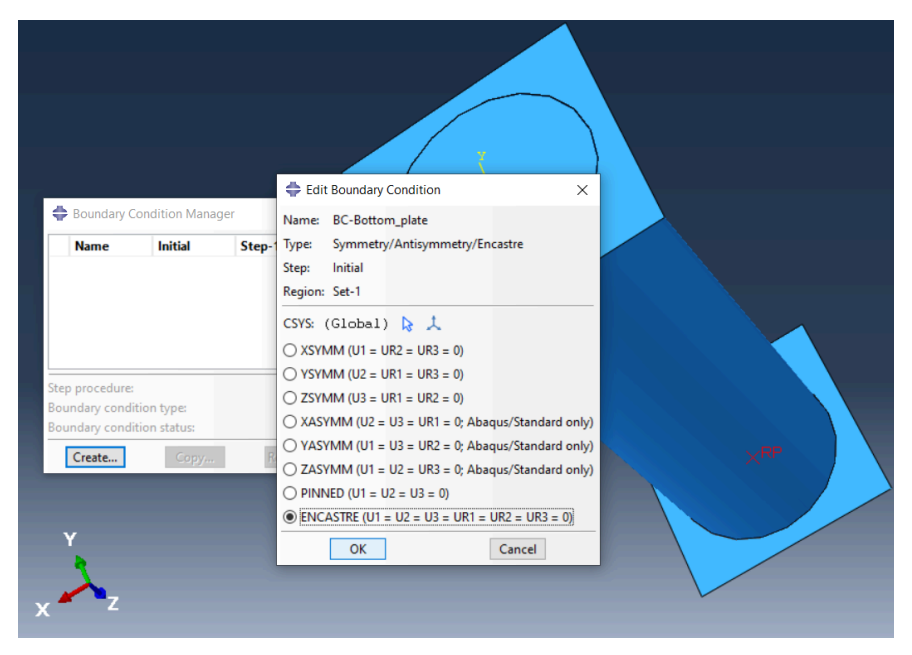


Fig 18. Bottom plate boundary conditions

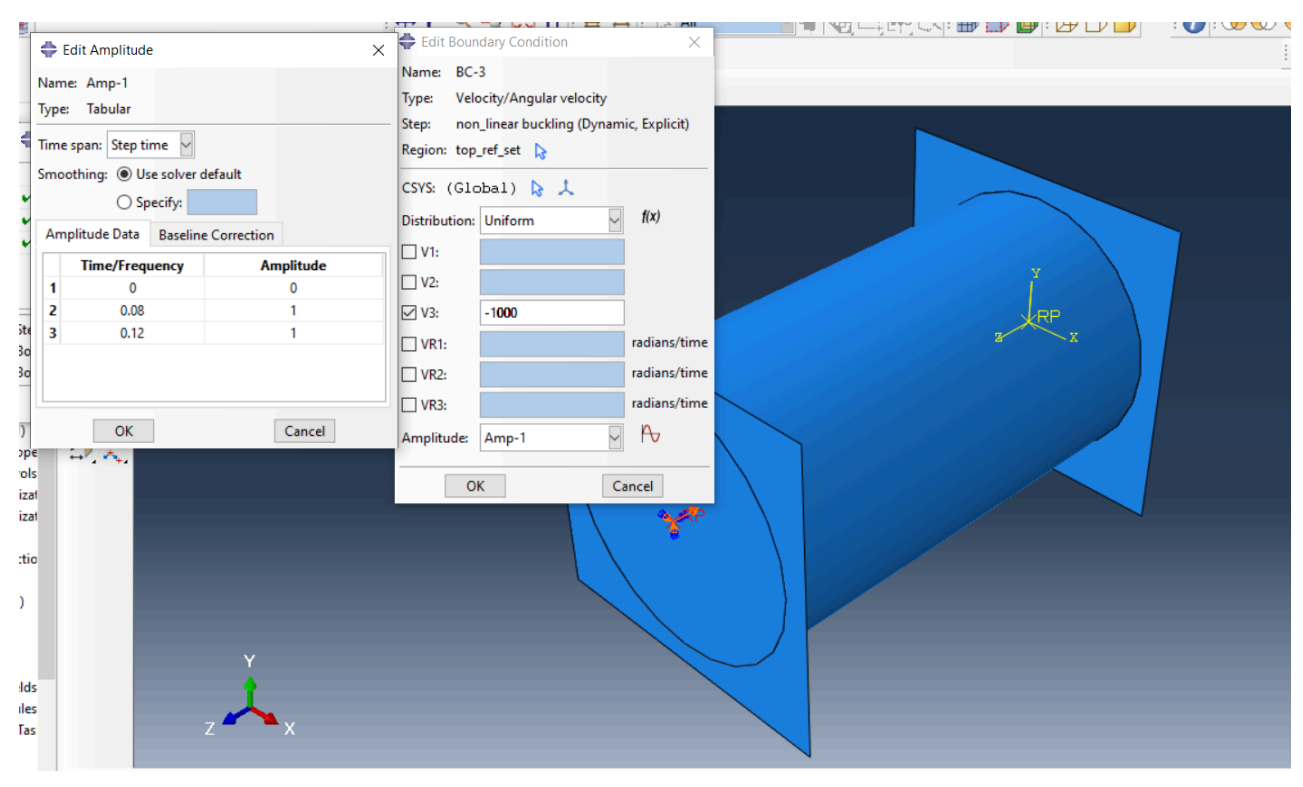


Fig 19. Applying load to the top plate (at reference point of the top plate)

# 4.4.9 Output Requests

Before submitting the job for the analysis, the desired outputs are to be specified by creating a "history output request" from the model tree. For this analysis, displacement of the top plate reference point in z direction and the reaction force from the bottom plate reference point in the z direction were chosen as our desired output. After the completion of the analysis, output of each simulation analysis can be seen in the "visualization" module. The complete simulation animation can also be seen by clicking on the "animate time history" button in the GUI which gives the shape of the deformation mode of the crash tube. The force-displacement curves for each sample were obtained by creating a new plot in the "XY Data" option which was the combination of the force vs time and displacement vs time curves.

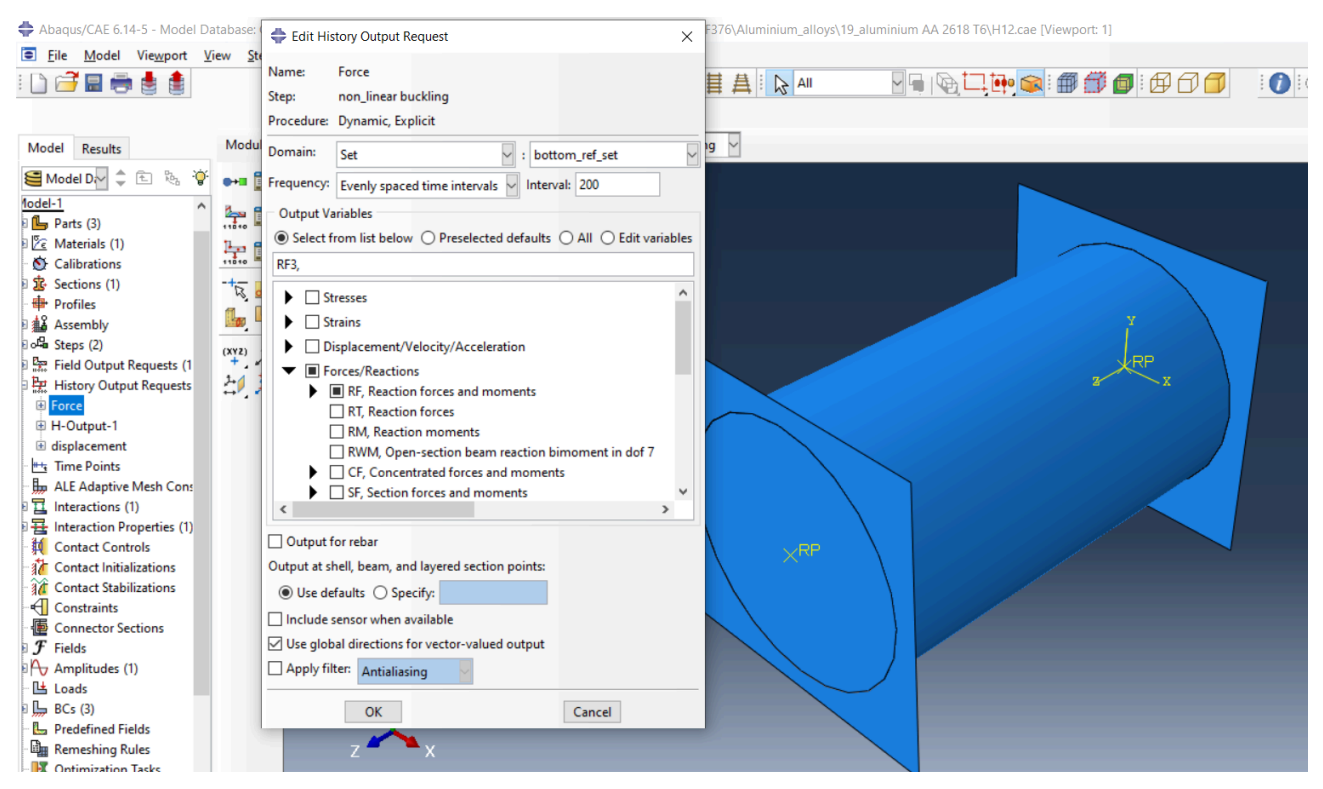


Fig 20. Selecting reaction force (from bottom plate reference point) as one of the history output request

# 5. Results and Discussions

All the aluminium samples mentioned earlier in the problem statement were considered for the simulation in abaqus/ explicit software and the respective force displacement curves were obtained thereafter for each of the samples. Again with the help of the software, uniaxial crushing simulations of all the samples were observed that revealed their crushing behaviour. Overall deformation modes shown by all the samples were more or less the same and most of them have shown concertina or ring mode (axisymmetric mode) of deformation under uniaxial quasi static compression, as depicted in Fig. 19. Very few samples have shown a different mode or rather a mixed mode of deformation like in the case of sample AA 2024 T4. The possible reason for similar mode of deformations in most of the samples could be the fact that the geometric and experimental parameters were kept constant throughout the analysis and their general mechanical properties such as elastic modulus, density and poisson's ratio were almost very similar which further limits the possibility of deviating from ring deformation mode.

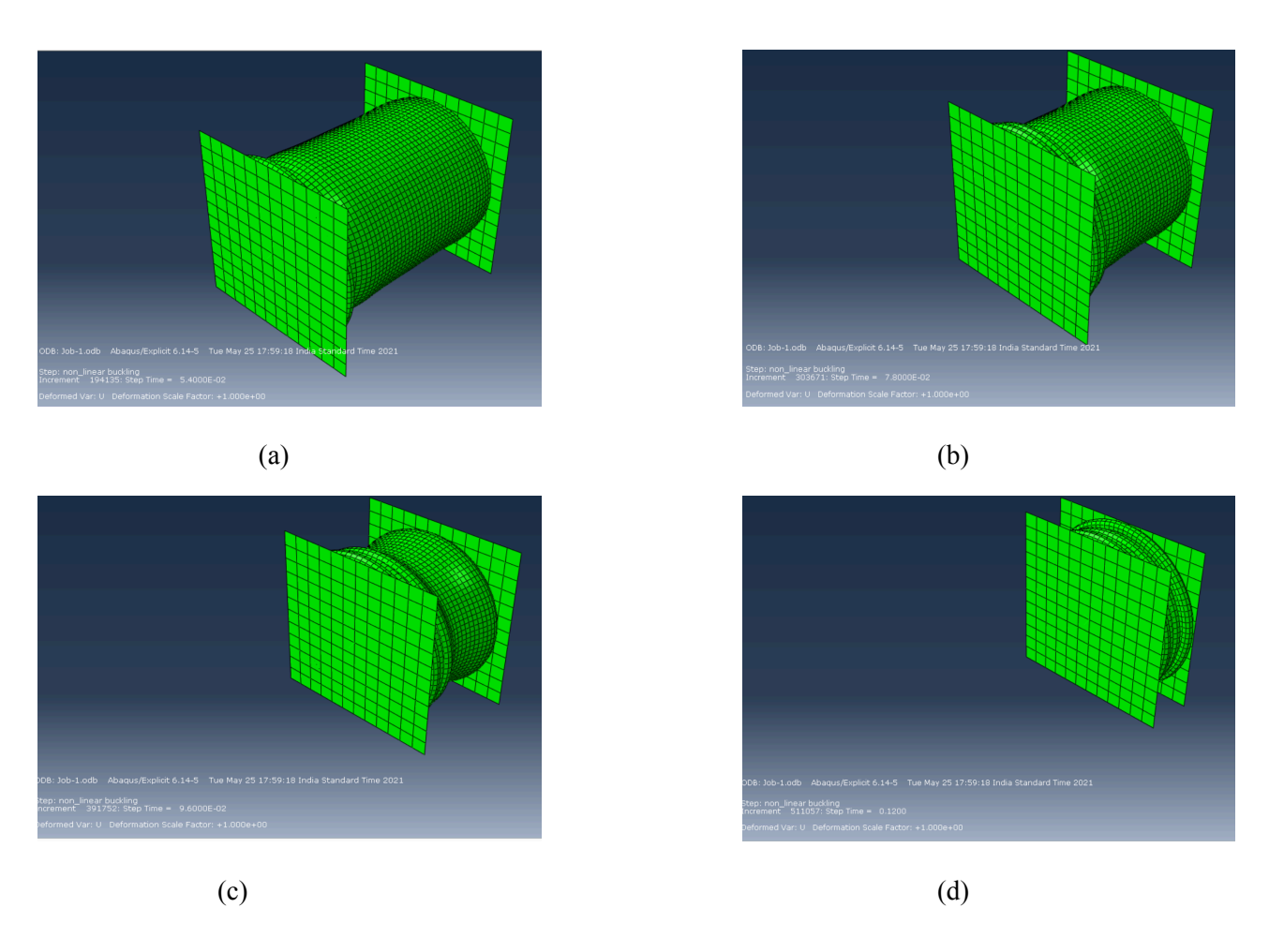


Fig. 21. Simulation of the crushing behaviour of AA 2024 O under uniaxial quasi static compression

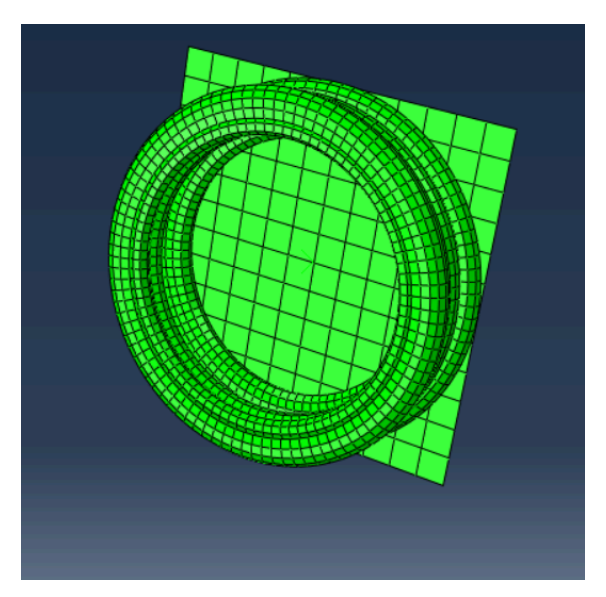


Fig .22. Deformation mode of AA 2024 O (Ring mode)

In order to assess the performance of each sample, the force displacement curves, as shown in Fig. 21, were analysed to yield some important parameters which would also help us in selection of the best aluminium alloy that could be used for the manufacturing of crash boxes. For this analysis, peak force, mean force, crush force efficiency, total energy absorption and specific energy absorption were taken as the main parameters.

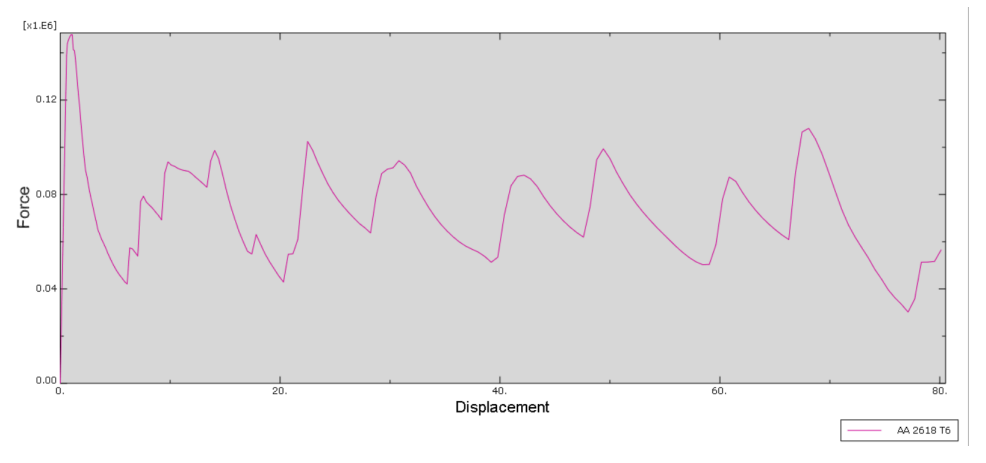


Fig 23. Force-displacement curve generated by operating on force and displacement curves (sample: AA 2618 T6)

Table No. 8 below shows the result for all the crash tubes which are tested. It gives the overall idea about the peak force, mean force, CFE, EA and SEA by the tube made up of different aluminium alloys compressed under the action of axial quasi-static load.

Table No. 8: Results of simulations of all aluminium samples

Sr. No.	Aluminum Grade	Peak Force (N)	Mean Force (N)	Crush Force Efficiency (%)	Energy Absorption (J)	Specific Energy Absorption (J/kg)
1	Pure Aluminum H12	34319.40	19178.13	55.88	1534.25	15041.67
2	Pure Aluminum H16	44742.20	23693.88	52.96	1895.51	18583.43
3	AA 1060 O	18415.70	13486.63	73.23	1078.93	10577.75
4	AA 1060 H12	29358.30	16358.13	55.72	1308.65	12829.90
5	AA 1060 H18	48053.60	25377.38	52.81	2030.19	19903.82
6	AA 1100 O	25614.40	18176.38	70.96	1454.11	14255.98
7	AA 1100 H14	45305.50	24440.63	53.95	1955.25	19169.12
8	AA 1100 H18	69646.20	35685.75	51.24	2854.86	27988.82
9	AA 2014 T6	177475.0	90308.50	50.89	7224.68	68545.35
10	AA 2021 O	44509.40	29350.25	65.94	2348.02	21842.05
11	AA 2021 T31	123751.0	70459.50	56.94	5636.76	52434.98
12	AA 2024 O	49332.00	30553.88	61.94	2444.31	23423.89
13	AA 2024 T3	146026.0	80017.25	54.80	6401.38	61344.61
14	AA 2024 T4	141484.0	76795.50	54.28	6143.64	58874.68
15	AA 2219 O	47241.40	30149.75	63.82	2411.98	22661.34
16	AA 2219 T31	125490.0	68357.25	54.47	5468.58	51379.09
17	AA 2219 T62	122113.0	70186.75	57.48	5614.94	52754.19
18	AA 2219 T851	145167.0	80424.50	55.40	6433.96	60449.15
19	AA 2618 T6	147706.0	72078.75	48.80	5766.30	55258.62
20	AA 3003 O	29390.60	20253.63	68.91	1620.29	15684.24
21	AA 3003 H12	47883.50	25580.00	53.42	2046.40	19808.94
22	AA 3003 H18	72375.50	36047.13	49.81	2883.77	27914.60
23	AA 3004 O	46699.00	30713.50	65.77	2457.08	24027.16
24	AA 3004 H32	72373.50	40419.43	55.85	3238.93	31754.22
25	AA 3004 H34	82219.10	44776.10	54.46	3588.07	34835.63

26	AA 3004 H38	98736.30	50331.27	50.98	4033.09	39156.21
27	AA 5050 O	38087.20	25611.58	67.24	2050.03	20297.33
28	AA 5050 H32	59831.30	32949.35	55.07	2640.33	26141.88
29	AA 5050 H34	67257.90	35997.55	53.52	2884.57	28560.10
30	AA 5050 H38	78459.00	40007.69	50.99	3205.80	31740.59
31	AA 5052 O	53336.20	33860.89	63.49	2714.59	26877.13
32	AA 5052 H34	88480.20	48576.27	54.90	3892.48	38539.41
33	AA 5052 H38	104390.00	55179.54	52.86	4421.68	43779.01
34	AA 5083 O	83570.80	51165.32	61.22	4100.65	40933.70
35	AA 5083 H12	121221.00	64816.81	53.47	5192.39	51831.72
36	AA 5083 H32	112115.00	63520.72	56.66	5089.96	50809.24
37	AA 5083 H34	124766.00	67497.42	54.10	5407.09	53983.89
38	AA 5086 O	75951.00	47573.29	62.64	3813.76	38069.89
39	AA 5086 H34	111129.00	63545.96	57.18	5092.16	50831.20
40	AA 5154 O	65340.40	41438.74	63.42	3322.04	33161.42
41	AA 5154 H32	91786.40	51130.53	55.71	4097.11	40898.36
42	AA 5154 H34	106735.00	57834.84	54.19	4633.86	46256.33
43	AA 5154 H38	116528.00	61456.37	52.74	4924.53	49157.87
44	AA 5454 O	68587.10	43679.40	63.68	3500.48	34942.65
45	AA 5454 H32	92070.30	51328.36	55.75	4113.84	41065.37
46	AA 5454 H34	108976.00	58392.07	53.58	4669.62	46613.30
47	AA 5456 O	92867.70	56197.02	60.51	4503.73	44911.71
48	AA 5456 H24	92643.80	57196.01	61.74	4481.01	44685.14
49	AA 5456 H321	97865.30	58952.79	60.24	4789.03	47756.75
50	AA 6061 O	34611.60	22621.98	65.36	1811.55	17714.69
51	AA 6061 T6	114150.0	59223.36	51.88	4746.93	46419.02
52	AA 6063 O	26952.30	14802.37	54.92	1383.12	13525.18
53	AA 6063 T4	64981.70	37447.35	57.63	3211.56	31405.03
54	AA 6063 T6	84417.00	45290.72	53.65	3629.63	35493.23
55	AA 6063 T832	103164.0	53080.11	51.45	4254.62	41604.84

56	AA 6066 O	44948.60	27344.13	60.83	2192.72	21442.05
57	AA 6066 T4	102410.0	58613.24	57.23	4697.98	45940.35
58	AA 6066 T6	137727.0	73876.23	53.64	5908.34	57776.15
59	AA X 7005 O	52019.90	33166.43	63.76	2659.49	25194.70
60	AA X 7005 T6	123481.0	65709.21	53.21	5268.86	49914.59
61	AA 7039 O	61685.70	38778.52	62.86	3109.77	29460.43
62	AA 7039 T6	147373.0	78097.91	52.99	6228.73	59007.93
63	AA 7075 O	61857.90	38353.84	62.00	3075.38	29134.64
64	AA 7075 T6	197269.0	98104.25	49.73	7872.16	74576.97
65	AA 7075 T73	167995.0	86311.21	51.38	6923.48	65589.65
66	AA 7079 O	61932.60	38398.63	62.00	3078.23	29800.21
67	AA 7079 T6	183061.0	92725.94	50.65	7435.61	71983.83
68	AA 7178 O	61981.0	38053.95	61.40	3051.31	28701.60
69	AA 7178 T6	196463.0	100974.72	51.4	8092.72	76122.72

To fulfil the aim of this analysis, a best suitable aluminium alloy was selected by making use of the "Technique for Order of Preference by Similarity to Ideal Solution" (TOPSIS) method. It is a multi-criteria decision analysis method which compares a set of alternatives by identifying weights for each criterion, normalising scores for each criterion and calculating the geometric distance between each alternative and the ideal alternative, that yields the best score in each criterion. Here, we took crush force efficiency and specific energy absorption as the 2 criterias on the basis of which the optimal alternative of all the selected aluminium alloys is determined. A clear step by step procedure is shown below which takes some of the 1000 series of Al in the analysis;

Table. 9. Aluminium alloys for TOPSIS analysis

Sr. No	Alloys	Crush force efficiency (%)	Specific energy absorption (J/ kg)
1	AA 1060 O	73.23438696	10577.7451
2	AA 1060 H12	55.71891084	12829.90196
3	AA 1060 H18	52.81055946	19903.82353
4	AA 1100 O	70.96154897	14255.98039

5	AA 1100 H14	53.9462648	19169.11765
6	AA 1100 H18	51.23861747	27988.82353

For crush force efficiency (CFE);

Denominator (D1) = 
$$\sqrt{\sum_{i=1}^{6} X_{1i}^{2}} = 147.7429$$
 (02)

Where  $X_{1\,i}$  are the crush force efficiency values corresponding to each sample

For Specific energy absorption;

Denominator (D2) = 
$$\sqrt{\sum_{i=1}^{6} X_{2i}^{2}} = 45019.10214$$
 (03)

Where  $X_{2i}$  are the Specific energy absorption values corresponding to each sample

Normalisation of each parameter (criteria) is carried out by individually dividing the respective denominator values as shown below;

Equal weightage is considered for both the parameters and so each of them were given 50 points. So the total points were chosen to be 100. Therefore,

Weight for CFE = 50/100 = 0.5

Weight for SEA = 50/100 = 0.5

The weighted normalised values were calculated by taking the product between the parameter weights and each normalised value.

Table 10. Normalised and weighted normalised values for each parameter

Sr. N o	Alloys	Normalised Crush force efficiency (%)	Normalised Specific energy absorption (J/ kg)	Weighted Normalised Crush force efficiency (%)	Weighted Normalised Specific energy absorption (J/ kg)
1	AA 1060 O	0.4957	0.2350	0.2478	0.1175
2	AA 1060 H12	0.3771	0.2850	0.1886	0.1425
3	AA 1060 H18	0.3574	0.4421	0.1787	0.2211
4	AA 1100 O	0.4803	0.3167	0.2402	0.1583
5	AA 1100 H14	0.3651	0.4258	0.1826	0.2129

6	AA 1100 H18	0.3468	0.6217	0.1734	0.3109
---	-------------	--------	--------	--------	--------

Deviation from the best alloys in each parameter (one that gives the maximum weighted normalised value in each parameter/criteria) is calculated for all the samples.

S+ represents the deviation from the best alternative and S- denotes the deviation from the worst alternative and are calculated as follows;

$$S_{i}^{+} = \sqrt{\sum_{j=1}^{2} (V_{ij} - V_{j}^{+})^{2}}$$
 (04)

$$S_{i}^{-} = \sqrt{\sum_{j=1}^{2} (V_{ij} - V_{j}^{-})^{2}}$$
 (05)

 $V_{j}^{+}$  and  $V_{j}^{-}$  represent the best and the worst weight normalised values in the jth parameter.

Finally, the probability of selection is calculated which becomes the basis for selecting the best alternative from those two chosen parameters. The sample with highest probability of selection was then considered to be the optimal alternative alloy which in this example comes out to be AA 1100 H18. The following table shows the probability of selection for each sample, from which it is clearly observed that sample No. 6 shows the highest probability of 0.72205 or 72.205 %.

Probability of selection (P) =  $S_i^- / (S_i^- + S_i^+)$ 

Table. 11. Deviation measurements and probability of selection for each sample

Sr. No	Alloys	$S_i^+$	$S_i^-$	Р
1	AA 1060 O	0.1934	0.0744	0.27795
2	AA 1060 H12	0.1785	0.0293	0.14080
3	AA 1060 H18	0.1133	0.1037	0.47788
4	AA 1100 O	0.1527	0.0783	0.33881
5	AA 1100 H14	0.1177	0.0959	0.44884
6	AA 1100 H18	0.0744	0.1934	0.72205

Determining the best suited material for crash box

Similar calculations are performed on the rest of the samples (including the above ones) to determine the best suited material for the crash box. The result for the same is shown in the Table below;

Table No. 12. Deviation measurements and probability of selection for all the samples in the analysis

1 y 515				
Sr. No.	Aluminum Grade	$S_i^+$	$S_i^-$	Р
1	Pure Aluminum H12	0.09011217374	0.009835770018	0.09840892817
2	Pure Aluminum H16	0.08581419483	0.01236154805	0.1259124473
3	AA 1060 O	0.09470630845	0.02561957886	0.2129182625
4	AA 1060 H12	0.09327775131	0.007951767674	0.07855186663
5	AA 1060 H18	0.08400601821	0.0141164974	0.1438660364
6	AA 1100 O	0.08942336153	0.02383665885	0.2104596023
7	AA 1100 H14	0.08474094069	0.01353613159	0.1377343798
8	AA 1100 H18	0.07327270866	0.02528708553	0.2565659328
9	AA 2014 T6	0.02586376086	0.08378628753	0.764124492
10	AA 2021 O	0.07880227378	0.02424770089	0.2353004061
11	AA 2021 T31	0.03825495881	0.06107860494	0.6148838583
12	AA 2024 O	0.07706088133	0.02311322996	0.2307305716
13	AA 2024 T3	0.02880354539	0.07362238443	0.7187865861
14	AA 2024 T4	0.0318760546	0.0700206209	0.6871727714
15	AA 2219 O	0.07787464774	0.02351364908	0.2319167972
16	AA 2219 T31	0.04080657757	0.05925343096	0.5921789517
17	AA 2219 T62	0.03759042895	0.06161646141	0.6210905431
18	AA 2219 T851	0.02936766971	0.07239122707	0.711399488
19	AA 2618 T6	0.03956240283	0.06455965197	0.6200382051
20	AA 3003 O	0.08744541585	0.02234123066	0.2034967946
21	AA 3003 H12	0.08397790131	0.01419142279	0.1445606651
22	AA 3003 H18	0.07386047088	0.02507235485	0.2534280676
23	AA 3004 O	0.07567901313	0.02634808246	0.2582459327
24	AA 3004 H32	0.06664945542	0.03147804178	0.3207871665
25	AA 3004 H34	0.06281971163	0.03554928298	0.3613870724
26	AA 3004 H38	0.05828891829	0.0413562073	0.4150349257

27	AA 5050 O	0.08090652821	0.02390080512	0.2280451602
28	AA 5050 H32	0.07468640022	0.02343030749	0.2388003841
29	AA 5050 H34	0.07176406155	0.0264504379	0.2693129634
30	AA 5050 H38	0.06823660084	0.03066464739	0.3100531888
31	AA 5052 O	0.07188557612	0.02813840317	0.281316574
32	AA 5052 H34	0.0576059611	0.04090535237	0.4152350723
33	AA 5052 H38	0.0513847413	0.04816120361	0.4838087946
34	AA 5083 O	0.05238095181	0.0457551925	0.4662420031
35	AA 5083 H12	0.04075891738	0.05980895489	0.5947123424
36	AA 5083 H32	0.04049529559	0.05871163439	0.5918098101
37	AA 5083 H34	0.03775927734	0.06296351203	0.6251168422
38	AA 5086 O	0.0560941894	0.04229016943	0.4298464709
39	AA 5086 H34	0.04023311426	0.05882283832	0.5938344621
40	AA 5154 O	0.06292214189	0.03605262643	0.3642607813
41	AA 5154 H32	0.05411219666	0.04440494284	0.4507331726
42	AA 5154 H34	0.04755160637	0.0518606301	0.5216725017
43	AA 5154 H38	0.04449425587	0.05589755811	0.5567939844
44	AA 5454 O	0.06033785772	0.03850936764	0.3895847102
45	AA 5454 H32	0.0538699034	0.04465038561	0.4532100551
46	AA 5454 H34	0.04735562651	0.05230898127	0.5248501192
47	AA 5456 O	0.04702800392	0.05110703528	0.5207827469
48	AA 5456 H24	0.04738948334	0.05074907774	0.5171165868
49	AA 5456 H321	0.04292761095	0.05523699764	0.5626976813
50	AA 6061 O	0.0847970102	0.02019457539	0.1923447034
51	AA 6061 T6	0.04840681019	0.05188805689	0.5173550592
52	AA 6063 O	0.09246319412	0.007702820169	0.07690053581
53	AA 6063 T4	0.06665260598	0.03148490928	0.3208243983
54	AA 6063 T6	0.06219272862	0.03635822168	0.3689281693
55	AA 6063 T832	0.05485509391	0.04491746511	0.4501985872
56	AA 6066 O	0.08007093954	0.02014081185	0.2009825351
57	AA 6066 T4	0.04672598415	0.05185534104	0.5260158649
58	AA 6066 T6	0.03353796124	0.06838584606	0.6709506628
59	AA X 7005 O	0.07425401304	0.02630631052	0.2615973138
60	AA X 7005 T6	0.04329669655	0.05702623235	0.5684267094
61	AA 7039 O	0.06829356615	0.03101430761	0.3123046183

62	AA 7039 T6	0.03258680524	0.07011510499	0.6827049743
63	AA 7075 O	0.06890694654	0.0301760721	0.3045534191
64	AA 7075 T6	0.02474299894	0.09247802222	0.7889201212
65	AA 7075 T73	0.02750960954	0.07953297154	0.7430031183
66	AA 7079 O	0.06796004669	0.03103256603	0.3134836547
67	AA 7079 T6	0.02441912042	0.08874729406	0.7842193681
68	AA 7178 O	0.06963414091	0.02932945576	0.2963661058
69	AA 7178 T6	0.02289621274	0.09474545679	0.8053732761

From the above calculations, sample no. 69 which is AA 7178 T6, came out to be the best alternative out of all the chosen samples. This also highlights the consequence of carrying out different heat treatment processes under varying conditions like temperature and time given for cooling of the material. It can also be observed that the probability of selection for most of the members from the 7000 series with T tempers showed more than 70% suggesting that Zinc being the alloying element in wrought aluminium would prove to give best the results in overall crashworthiness of a vehicle. It also suggests that obtaining final alloy products by solution heat treatment with or without supplementary strain hardening can prove to be an advantage in having optimal crushing performance over all other heat treatment processes carried out on wrought aluminium grades. Most of the T-tempers in all the series have shown somewhat optimal crushing characteristics judging by their respective probability values.

#### 6. References

- [1] Zheng, G., Fan, Z., Zhang, H. *et al.* Crashworthiness Optimization of Steel–Magnesium Hybrid Double-Hat-Shaped Tubes. *Automot. Innov.* 1, 247–254 (2018). https://doi.org/10.1007/s42154-018-0033-9
- [2] Lakshmana Rao, C.\_ Narayanamurthy, V.\_ Simha, K. R. Y-Applied impact mechanics-Wiley (2016).
- [3] X. Zhang and H. Zhang, "Experimental and numerical investigation on crush resistance of polygonal columns and angle elements," Thin-Walled Struct., vol. 57, pp. 25–36, 2012, doi: 10.1016/j.tws.2012.04.006.
- [4] A. Alavi Nia and M. Parsapour, "Comparative analysis of energy absorption capacity of simple and multi-cell thin-walled tubes with triangular, square, hexagonal and octagonal sections," Thin-Walled Struct., vol. 74, pp. 155–165, 2014, doi: 10.1016/j.tws.2013.10.005.
- [5] Z. Fan, G. Lu, and K. Liu, "Quasi-static axial compression of thin-walled tubes with different cross-sectional shapes," Eng. Struct., vol. 55, pp. 80–89, 2013, doi: 10.1016/j.engstruct.2011.09.020.
- [6] S. Ming, Z. Song, T. Li, K. Du, C. Zhou, and B. Wang, "The energy absorption of thin-walled tubes designed by origami approach applied to the ends," Mater. Des., vol. 192, p. 108725, 2020, doi: 10.1016/j.matdes.2020.108725.
- [7] A. A. Nia and J. H. Hamedani, "Comparative analysis of energy absorption and deformations of thin walled tubes with various section geometries," Thin-Walled Struct., vol. 48, no. 12, pp. 946–954, 2010, doi: 10.1016/j.tws.2010.07.003.
- [8] J. Song, Y. Chen, and G. Lu, "Light-weight thin-walled structures with patterned windows under axial crushing," Int. J. Mech. Sci., vol. 66, pp. 239–248, 2013, doi: 10.1016/j.ijmecsci.2012.11.014.
- [9] A. K. Lakshminarayanan and C. J. Daniel, "Influence of friction stir welding variants on crashworthiness of friction stir welded aluminium top hat sections," Mater. Sci. Forum, vol. 979 MSF, pp. 97–101, 2020, doi: 10.4028/www.scientific.net/MSF.979.97.
- [10] F. Tarlochan, F. Samer, A. M. S. Hamouda, S. Ramesh, and K. Khalid, "Design of thin wall structures for energy absorption applications: Enhancement of crashworthiness due to axial and oblique impact forces," Thin-Walled Struct., vol. 71, pp. 7–17, 2013, doi: 10.1016/j.tws.2013.04.003.
- [11] K. Yang, "Design Optimization of Energy Absorption Structures with Origami Patterns A thesis submitted in fulfilment of the requirements for the degree of Doctor of Philosophy," no. February, 2018.

- [12] Z. Yang, Y. Yu, Y. Wei, and C. Huang, "Crushing behavior of a thin-walled circular tube with internal gradient grooves fabricated by SLM 3D printing," Thin-Walled Struct., vol. 111, no. November 2016, pp. 1–8, 2017, doi: 10.1016/j.tws.2016.11.004.
- [13] K. Yang, S. Xu, S. Zhou, J. Shen, and Y. M. Xie, "Design of dimpled tubular structures for energy absorption," Thin-Walled Struct., vol. 112, no. December 2016, pp. 31–40, 2017, doi: 10.1016/j.tws.2016.12.003.
- [14] R. yang Yao, G. sheng Yin, W. qian Hao, Z. yu Zhao, X. Li, and X. li Qin, "Axial buckling modes and crashworthiness of circular tube with external linear gradient grooves," Thin-Walled Struct., vol. 134, no. October 2018, pp. 395–406, 2019, doi: 10.1016/j.tws.2018.10.022.
- [15] M. D. Goel, "Numerical investigation of the axial impact loading behaviour of single, double and stiffened circular tubes," Int. J. Crashworthiness, vol. 21, no. 1, pp. 41–50, 2016, doi: 10.1080/13588265.2015.1113617.
- [16] S. Montazeri, M. Elyasi, and A. Moradpour, "Investigating the energy absorption, SEA and crushing performance of holed and grooved thin-walled tubes under axial loading with different materials," Thin-Walled Struct., vol. 131, no. December 2014, pp. 646–653, 2018, doi: 10.1016/j.tws.2018.07.024.
- [17] C. W. Isaac and O. Oluwole, "Structural response and performance of hexagonal thin-walled grooved tubes under dynamic impact loading conditions," Eng. Struct., vol. 167, no. April, pp. 459–470, 2018, doi: 10.1016/j.engstruct.2018.04.053.
- [18] M. Kamran, X. Pu, N. Ahmed, and A. A. G. Hanif, "Effect of semi-apical angle on the crush mechanics of metallic bi-tubular tubes under dynamic axial loading," Rev. Mater., vol. 24, no. 1, 2019, doi: 10.1590/s1517-707620190001.0628.
- [19] W. Liu, Z. Lin, N. Wang, and X. Deng, "Dynamic performances of thin-walled tubes with star-shaped cross section under axial impact," Thin-Walled Struct., vol. 100, pp. 25–37, 2016, doi: 10.1016/j.tws.2015.11.016.
- [20] W. Liu, L. Jin, Y. Luo, and X. Deng, "Multi-objective crashworthiness optimisation of tapered star-shaped tubes under oblique impact," Int. J. Crashworthiness, vol. 0, no. 0, pp. 1–15, 2020, doi: 10.1080/13588265.2020.1717917.
- [21] A. Rahi, "Controlling energy absorption capacity of combined bitubular tubes under axial loading," Thin-Walled Struct., vol. 123, no. October 2017, pp. 222–231, 2018, doi: 10.1016/j.tws.2017.11.032.
- [22] M. R. U. Rahim, P. K. Bharti, A. A. Azmi, and A. Umer, "Axial crushing comparison of sinusoidal thin-walled corrugated tubes," Mater. Today Proc., vol. 5, no. 9, pp. 19431–19440, 2018, doi: 10.1016/j.matpr.2018.06.304.
- [23] Q. Estrada et al., "Effect of radial clearance and holes as crush initiators on the crashworthiness performance of bi-tubular profiles," Thin-Walled Struct., vol. 140, no. March, pp. 43–59, 2019, doi: 10.1016/j.tws.2019.02.039.
- [24] Ministry of Road Transport and Highways (2020, January 17), *Traffic Accidents (Chapter 1 A)* https://ncrb.gov.in/sites/default/files/Chapter-1A-Traffic-Accidents 2019.pdf